# Cryptic Variations in Abyssal Peridotite Compositions: Evidence for Shallow-level Melt Infiltration in the Oceanic Lithosphere

## J. M. WARREN[1,2]* AND N. SHIMIZU[3]

[1]MIT/WHOI JOINT PROGRAM, WOODS HOLE OCEANOGRAPHIC INSTITUTION, WOODS HOLE, MA 02543, USA

[2]DEPARTMENT OF TERRESTRIAL MAGNETISM, CARNEGIE INSTITUTION OF WASHINGTON, 5241 BROAD BRANCH ROAD, NW, WASHINGTON, DC 20015, USA

[3]DEPARTMENT OF GEOLOGY AND GEOPHYSICS, WOODS HOLE OCEANOGRAPHIC INSTITUTION, WOODS HOLE, MA 02543, USA

*Ranges in clinopyroxene trace element contents of 2–3 orders of magnitude occur over <2 cm distance in peridotite samples from the Atlantis II Fracture Zone on the Southwest Indian Ridge. This represents the smallest length-scale at which clinopyroxene trace element concentrations have been observed to vary in abyssal peridotites. Because of the absence of any accompanying veins or other macroscopic features of melt–rock interaction, these peridotites are interpreted as being the result of cryptic metasomatism by a low-volume melt. The small length-scale of the variations, including porphyroclastic clinopyroxene grains of 2 mm diameter with an order of magnitude variation in light rare earth elements, precludes an ancient origin for these anomalies. Calculation of diffusive homogenization time-scales suggests that for the trace element variations to be preserved, metasomatism occurred in the oceanic lithospheric mantle at 1000–1200°C and 10–20 km depth. This observation provides constraints for the on-axis thickness of the lithospheric mantle at an ultraslow-spreading ridge. Trace amounts of plagioclase are present in at least two of the metasomatized samples. Textural and trace element observations indicate that it formed following the trace element metasomatism, indicating that the mantle can be infiltrated multiple times by melt during the final stages of uplift at the ridge axis. The peridotites in this study are from two oceanic core complexes on the Atlantis II Fracture Zone. Our observations of multiple late-stage metasomatic events in the lithospheric mantle agree with current models and observations of melt intrusion into the mantle during oceanic core complex formation. These observations also indicate that heterogeneous lithospheric mantle can be created at ultraslow-spreading ridges.*

## INTRODUCTION

Melting, melt transport and melt extraction at mid-ocean ridges are complex processes. Adiabatically ascending basaltic melts beneath mid-ocean ridges are known to react with and crystallize in wall-rock mantle peridotites (Kelemen *et al.*, 1992; Seyler *et al.*, 2001; Brunelli *et al.*, 2006). For example, porous melt flow results in replacive dunite formation via the dissolution of pyroxene and precipitation of olivine (e.g. Kelemen *et al.*, 1995). Dunites have been observed from all ridge systems (Constantin *et al.*, 1995; Dick & Natland, 1996; Ghose *et al.*, 1996; Dick *et al.*, 2003, 2010) and in ophiolites such as Trinity, Internal Ligurides, Oman, Josephine and Bay of Islands (Kelemen *et al.*, 1992; Hoogerduijn Strating *et al.*, 1993; Boudier & Nicolas, 1995; Kelemen & Dick, 1995; Suhr *et al.*, 2003). In addition to dunites, melt migration results in a large variety of vein lithologies that crystallize over a range of depths in the mantle, as demonstrated by Python &

*Corresponding author. E-mail: jwarren@dtm.ciw.edu

Ceuleneer (2003) from a survey of veins in the Oman Ophiolite. Among abyssal ultramafic samples, the formation of websterites and olivine websterites by the crystallization of trapped melts at depth has been documented at the Mid-Atlantic Ridge (MAR) and Southwest Indian Ridge (SWIR) (Dick *et al.*, 1984; Fujii, 1990; Juteau *et al.*, 1990; Dantas *et al.*, 2007; Warren *et al.*, 2009).

In addition to reactive dunite formation and melt crystallization, melt flow through the mantle results in more cryptic forms of melt–rock reaction, often referred to as metasomatism. Mantle metasomatism has received widespread attention in the orogenic, ophiolite and xenolith literature (e.g. Menzies *et al.*, 1987; Bodinier *et al.*, 1990; Van der Wal & Bodinier, 1996; Le Roux *et al.*, 2007; Hanghøj *et al.*, 2010). However, metasomatism in these types of peridotites often relates to processes in the sub-continental lithospheric mantle. In abyssal peridotites, metasomatism is a direct result of the processes at mid-ocean ridges that also result in the formation of oceanic crust.

Typically, abyssal peridotites have been treated as the depleted residues of mantle melting (e.g. Johnson *et al.*, 1990), but more recent observations have recognized the importance of metasomatism beneath ridges. Seyler *et al.* (2001, 2007) presented textural evidence for the crystallization of clinopyroxene (Cpx), spinel and sulfide in peridotites as a result of incomplete melt extraction at ridges. Asthenospheric metasomatism by an enriched mantle component has been identified at the SWIR on the basis of orthopyroxene (Opx) mineral inclusions with unusual mineralogy and high incompatible element concentrations (Seyler *et al.*, 2004). From trace element modeling, Brunelli *et al.* (2006) argued for weak refertilization of the mantle by low-degree, partially aggregated melts, based on elevations in peridotite Cpx incompatible element concentrations. At the Romanche Fracture Zone on the MAR, peridotites contain up to 16% plagioclase, indicating regional-scale melt–rock interaction in the mantle (Seyler & Bonatti, 1997; Tartarotti *et al.*, 2002). Dick *et al.* (2010) found evidence at Kane Megamullion on the MAR for at least two types of metasomatism, in the form of variable alumina depletion in pyroxene rims in some residual peridotites and small amounts of plagioclase in others. Hence, melt migration through the shallow upper mantle can result in a variety of products, the results of which are diverse and reflect the conditions under which they occur.

In this study, we present a detailed analysis of centimeter- to sub-centimeter-scale melt–mantle interaction in peridotites from the SWIR. Our results further document the types of melt–mantle reactions that occur at ridges and provide constraints on the length-scales and magnitudes of these reactions. Peridotites in this study are from an ultraslow-spreading environment (ridge full spreading rate <20 mm/year), where conductive cooling results in the cessation of melting at depth and the formation of a thinner basaltic crust (e.g. Bown & White, 1994; Dick *et al.*, 2003; Montési & Behn, 2007). Conductive cooling should result in both less depleted residual mantle and a greater potential for diverse reactions between ascending melts and wall-rock peridotite. In contrast, peridotites from the fast-spreading East Pacific Rise (EPR) are highly depleted by melting, except where late melt fractions have locally reacted with the surrounding peridotite (Cannat *et al.*, 1990; Dick & Natland, 1996; Constantin, 1999).

Peridotites in this study are from two locations on the eastern side of the Atlantis II Fracture Zone on the SWIR (Fig. 1): the inside-corner high at the northern ridge–transform intersection (RTI) and a fossil inside-corner high located at 12 Ma along the fracture zone, known as Atlantis Bank (Dick *et al.*, 1991; Baines *et al.*, 2003, 2009; John *et al.*, 2004). The full spreading rate in this area is 14·1 mm/year, but as a result of asymmetrical spreading, the half-spreading rate to the south is 8·7 mm/year (Hosford *et al.*, 2003; Baines *et al.*, 2007). During the formation of Atlantis Bank, Baines *et al.* (2008) estimated both a faster full spreading rate of 15·7 km/year and highly asymmetrical spreading that resulted in a half-spreading rate to the south of 14·1 mm/year. Both Atlantis Bank and the current RTI are oceanic core complexes, exposed sections of lower crust and upper mantle that are exhumed by low-angle detachment faulting at the ridge axis (Cann *et al.*, 1997; Tucholke *et al.*, 1998).

Previous work on peridotites from the Atlantis II Fracture Zone by Johnson & Dick (1992) and Coogan *et al.* (2004) investigated temporal variations in melt productivity, based on spatial variations in peridotite composition along the entire fracture zone. Peridotite Cpx trace element concentrations were used as a measure of melt depletion. Overall, light rare earth elements (LREE) were found to vary by approximately an order of magnitude along the fracture zone. In this study, vein-free spinel peridotites from the fracture zone are found to have 2–3 orders of magnitude variation in Cpx trace element concentrations. The large variations in trace elements at the centimeter-scale are demonstrated to indicate late-stage melt–rock reaction at the ridge. The role of metasomatism in the context of oceanic core complex formation is then discussed.

## METHODS

We analyzed 14 peridotites from two dredges and five submersible dives from the Atlantis II Fracture Zone, as shown in Fig. 1 and Table 1. Peridotites were analyzed for mineral modes and major and trace element compositions, combined with thin-section petrography. Data for some peridotites from dredge RC27-9-6 are from Lee (1997) and are indicated as such in the tables. Modal analyses, given in Table 2, were made by point counting a minimum
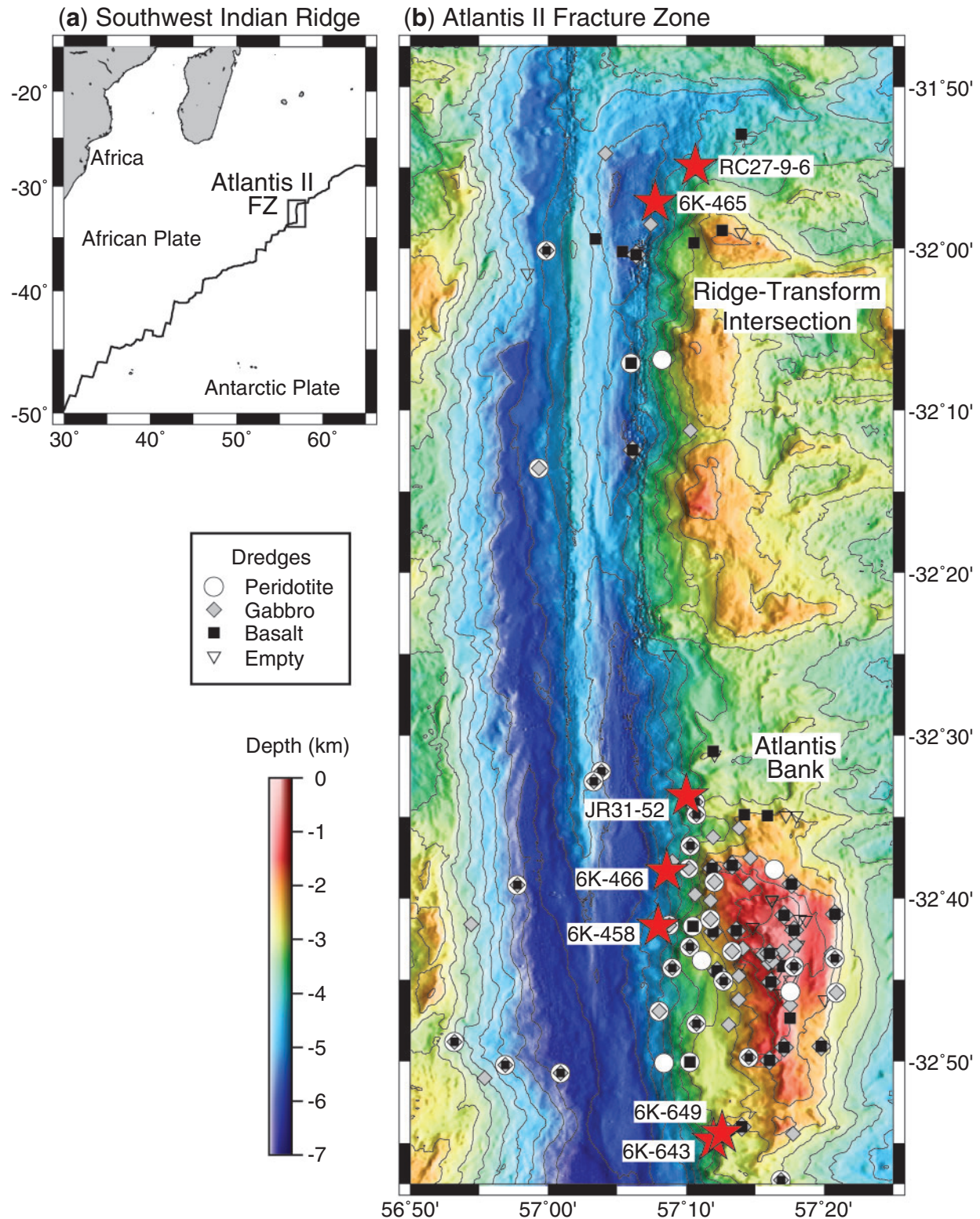
**Fig. 1.** Map of the Atlantis II Fracture Zone indicating locations of samples (red stars) used in this study. Samples are from the active ridge–transform intersection and from Atlantis Bank, located at 12 Ma along the fracture zone. Spreading is asymmetrical, with a half-spreading rate to the south of 8·7 mm/year and a full spreading rate of 14·1 mm/year (Hosford *et al.*, 2003; Baines *et al.*, 2007). Baines *et al.* (2008) estimated that from 10·3 to 12·7 Ma, during the formation of Atlantis Bank, the full spreading rate was higher (15·7 mm/year) and more asymmetrical, with a half-spreading rate to the south of 14·1 mm/year.

*Table 1: Atlantis II Fracture Zone sample locations*

| Dredge/dive | Outcrop type | Wt (kg) | Lat. (°S) | Long. (°E) | Depth (m) | Locality |
|---|---|---|---|---|---|---|
| *R.V.* Conrad, *1986* | | | | | | |
| RC27-9-6 | Dredge | 37 | −31·92 | 57·18 | 3930 | AIIFZ RTI† |
| *R.R.S.* James Clark Ross, *1998* | | | | | | |
| JR31-52 | Dredge | 125 | −32·56 | 57·17 | 3200 | Atlantis Bank |
| *R.V.* Yokosuka, Shinkai 6500 *submersible, 1998* | | | | | | |
| 6K-458-1 | Float in sediment | 3 | −32·69 | 57·13 | 4867 | Atlantis Bank |
| 6K-458-3 | On outcrop | 8 | −32·69 | 57·13 | 4609 | Atlantis Bank |
| 6K-465-2 | Float in sediment | 10 | −31·95 | 57·13 | 4988 | AIIFZ RTI |
| 6K-466-1 | Float in sediment | 3 | −32·64 | 57·14 | 4714 | Atlantis Bank |
| *R.V.* Yokosuka, Shinkai 6500 *submersible, 2001* | | | | | | |
| 6K-643-1 | From outcrop | 9 | −32·91 | 57·20 | 3396 | Atlantis Bank |
| 6K-643-6 | On outcrop | 2 | −32·91 | 57·21 | 2974 | Atlantis Bank |
| 6K-643-13 | Talus | 13 | −32·91 | 57·21 | 2712 | Atlantis Bank |
| 6K-649-5 | From outcrop | 3 | −32·91 | 57·21 | 2564 | Atlantis Bank |

†Ridge–transform intersection.

*Table 2: Sample descriptions and modal analyses*

| Sample | Loc.* | Description | Oliv | Opx | Cpx | Spin | Plag | Total | Points† |
|---|---|---|---|---|---|---|---|---|---|
| RC27-9-6-5‡ | RTI | Lherz, cryptic metasomatism | | | | | | | |
| RC27-9-6-7 | RTI | Lherzolite | | | | | | | |
| JR31-52-3 | AB | Harzburgite | 57·6 | 37·5 | 3·9 | 1·0 | 0·00 | 100·0 | 2056 |
| JR31-52-4 | AB | Lherzolite | | | | | | | |
| JR31-52-5 | AB | Harzburgite | 66·8 | 27·3 | 4·5 | 1·4 | 0·00 | 100·0 | 2258 |
| JR31-52-8 | AB | Lherzolite | 62·8 | 29·9 | 6·5 | 0·8 | 0·00 | 100·0 | 1975 |
| 6K-458-1 | AB | Perid, cryptic metasomatism | | | | | | | |
| 6K-458-3 | AB | Perid, cryptic metasomatism | | | | | | | |
| 6K-465-2‡ | RTI | Lherz, cryptic metasomatism | 71·0 | 22·0 | 5·9 | 1·1 | 0·01 | 100·0 | 1926 |
| 6K-466-1 | AB | Harzburgite | 74·8 | 21·2 | 3·0 | 1·1 | 0·00 | 100·0 | 1489 |
| 6K-643-1§ | AB | Lherzolite | 74 | 17 | 9 | 0·5 | | 100·5 | |
| 6K-643-6§ | AB | Harzburgite | 75 | 21 | 3 | 0·5 | | 99·5 | |
| 6K-643-13 | AB | Lherzolite | 68·7 | 24·9 | 5·1 | 0·7 | 0·00 | 99·4 | 1566 |
| 6K-649-5§ | AB | Lherzolite | 71 | 19 | 9 | 0·5 | | 99·5 | |

*Location is either the ridge–transform intersection (RTI) or Atlantis Bank (AB).
†Points counted on 51 mm × 75 mm thin sections using a 1 mm grid.
‡Contains trace amounts of plagioclase (<0·01%).
§Modal analysis from Morishita *et al.* (2007).

of 1400 points on large (51 mm × 75 mm) thin sections at 1 mm intervals. Alteration pseudomorphs of primary phases were included in the counts of primary mineral phases (olivine, orthopyroxene, Cpx, and spinel).

Silicate and oxide major element compositions were measured on the Massachusetts Institute of Technology JEOL JXA-733 Superprobe using wavelength-dispersive spectroscopy, a 15 kV accelerating potential and a 10 nA

beam current. Peak counting times were either 20 s or 40 s, except for Fe in pyroxenes, for which the time was 60 s. Data were reduced using matrix corrections (Bence & Albee, 1968) with modifications (Albee & Ray, 1970). For pyroxenes, a defocused beam spot size of 10 μm was used for ~10 analyses per 100 μm traverse to obtain bulk grain analyses that incorporate the effects of exsolution lamellae (Tables 3 and 4). Olivine, spinel and plagioclase were analyzed using a focused beam and averaging 6 analyses per grain (Tables 5, 6 and 7). Using the same electron microprobe and similar analytical procedures for basaltic glass, Gaetani & Grove (1998) used repeat analyses to estimate analytical reproducibility: elements at >10 wt % levels are reproducible within 2%, elements at <10 wt % levels are reproducible within 5% and elements at <1 wt % level are reproducible within 30%.

Abundances of Na, Ti, Cr, Sr, Y, Zr and REE (La, Ce, Nd, Sm, Eu, Dy, Er, Yb) in Cpx (Tables 8 and 9) and plagioclase (Table 10) were determined by secondary ion mass spectrometry using the Cameca IMS-3f at Woods Hole Oceanographic Institution, following the technique of Johnson et al. (1990). Samples were ionized using a primary beam of $O^-$ with an accelerating voltage of −8·30 kV and a current of 6–7 nA. The beam was focused to an ~10 μm spot diameter for REE and an ~4 μm spot for other trace elements, with the trace element analytical spot positioned adjacent to the REE analysis spot. The energy filtering technique of Shimizu et al. (1978) was used to suppress molecular ion interferences, with a high voltage offset of 60 V for REE and 90 V for other elements. Working curves relating secondary ion intensity to concentration were determined using Cpx from the standard KH1 (Kilbourne Hole peridotite; Irving & Frey, 1984) for REE and basalt glass standard KL2G (Kilauea tholeiite; Jochum et al., 2000) for other trace elements. Standards were typically measured two or more times per session and the average value of all standard analyses per session was used to calculate session-specific working curves.

Data were collected in five count cycles with count times of 30 s for REE and 5–20 s for other trace elements. For REE, $^{30}Si$ was measured at the start and end of each analysis, with the time interpolated average used to calculate REE/Si ratios, for determination of concentrations from the working curves. For the other trace elements, $^{28}Si$ was measured during each cycle, with the average value after all cycles used to determine concentrations. Traditionally, within-cycle ratios of REE/Dy and trace element/Si are used to account for temporal variability in peak intensities (e.g. Johnson et al., 1990; Johnson & Dick, 1992). Because of random background noise that produced occasional extremely high counts (1–3 orders of magnitude above the number of counts from the other cycles), this ratio scheme was abandoned. However, the error introduced by temporal variability in peak intensity is insignificant compared

with primary beam instability, which cannot be monitored on the IMS-3f.

Low count rates among REE are best treated statistically by a Poisson distribution, with the standard deviation given by $\sqrt{\bar{x}}$, where $\bar{x}$ is the five-cycle raw count average for an element. To remove the effects of the random background noise, any single REE count greater than $3\sqrt{\bar{x}}$ away from the median count value was discarded. After recalculating $\bar{x}$, any count more than $2\sqrt{\bar{x}}$ from the average count value was discarded. For the other trace elements, which have higher count rates, any count greater than two standard deviations from the median count value was discarded. After a final re-averaging of counts, element ratios to Si were calculated and concentrations derived from working curves.

Trace element analyses in abyssal peridotites are difficult because of their low concentrations, particularly for REE. We assessed data quality from measurements of an independent standard, sample count statistics, sample duplicate analyses, and REE pattern shape. All data were checked for the smoothness of their REE patterns and analyses with irregular patterns that were not reproduced by repeat analysis were discarded. REE measured in an independent standard, Cpx from KLB-1 (Kilbourne Hole lherzolite; Takahashi, 1986, with trace element data by E. Nakamura, personal communication), provide an estimate of analytical reproducibility. From 21 analyses over 15 months, KLB-1 Cpx had a reproducibility of 9–17%, depending on the element (Table 8). Analytical error can also be estimated from the count statistics of each analysis and by comparison of duplicate analyses (Table 8). The average per cent error in concentration based on the counting error ranges from 0·2 to 21% (Table 8), with LREE having the largest errors. The error based on the average difference between 35 pairs of duplicate analyses is also given in Table 8, based on data in this study and our unpublished dataset. The average deviation among duplicate analyses of Cpx ranges from 7 to 37%. We conclude that the error among duplicate analyses of Cpx provides the best measure of REE error. A comparative study by Hellebrand et al. (2002) of analytical conditions between the WHOI IMS-3f and the Max-Planck-Institute for Chemistry, Mainz IMS-3f demonstrated reproducibility of REE patterns within analytical error. Overall, despite the large errors, the ion probe provides useful and interpretable data because of the orders of magnitude variation in trace element concentrations and the overall smoothness and reproducibility of REE patterns.

# RESULTS
## Description of the peridotites
The peridotites in this study are classified into two groups on the basis of their REE concentrations: residual peridotites and cryptically metasomatized peridotites

*Table 3: Major element compositions of Cpx (in wt %)*

| Analysis | Grn* | Pts | $SiO_2$ | ± | $TiO_2$ | ± | $Al_2O_3$ | ± | $Cr_2O_3$ | ± | FeO | ± | MnO | ± | MgO | ± | CaO | ± | $Na_2O$ | ± | Total | Wo | En | Mg-no. | Cr-no. | Notes† |
|---|---|---|---|---|---|---|---|---|---|---|---|---|---|---|---|---|---|---|---|---|---|---|---|---|---|---|
| 6K-458-1 | 1C | 9 | 51·38 | 0·76 | 0·23 | 0·02 | 5·69 | 1·19 | 1·50 | 0·13 | 2·20 | 0·11 | 0·10 | 0·02 | 15·70 | 0·38 | 23·12 | 0·29 | 0·53 | 0·04 | 100·44 | 49·5 | 46·8 | 92·7 | 15·0 | Enr |
| 6K-458-1 | 1R | 8 | 52·36 | 1·81 | 0·26 | 0·08 | 5·28 | 1·34 | 1·35 | 0·26 | 2·77 | 1·42 | 0·10 | 0·03 | 18·77 | 6·48 | 19·69 | 8·07 | 0·48 | 0·20 | 101·05 | 41·1 | 54·4 | 92·4 | 14·6 | Enr |
| 6K-458-1 | 2I | 9 | 51·92 | 0·59 | 0·33 | 0·03 | 5·37 | 0·72 | 1·25 | 0·05 | 2·22 | 0·13 | 0·10 | 0·03 | 16·47 | 0·30 | 22·77 | 0·88 | 0·50 | 0·07 | 100·93 | 48·0 | 48·3 | 93·0 | 13·5 | Enr |
| 6K-458-1 | 3I | 9 | 52·43 | 0·48 | 0·31 | 0·05 | 4·14 | 0·60 | 1·56 | 0·13 | 2·21 | 0·13 | 0·10 | 0·03 | 16·51 | 0·26 | 23·24 | 0·19 | 0·48 | 0·03 | 100·98 | 48·5 | 47·9 | 93·0 | 20·2 | Enr |
| 6K-458-3 | 1I | 10 | 52·09 | 0·34 | 0·32 | 0·02 | 4·71 | 0·22 | 0·80 | 0·02 | 2·51 | 0·15 | 0·09 | 0·01 | 15·97 | 0·15 | 22·54 | 0·55 | 0·41 | 0·04 | 99·43 | 48·3 | 47·6 | 91·9 | 10·2 | |
| 6K-458-3 | 2I | 12 | 52·21 | 0·28 | 0·27 | 0·01 | 5·66 | 0·19 | 0·95 | 0·05 | 2·53 | 0·18 | 0·09 | 0·02 | 15·66 | 0·39 | 22·73 | 0·69 | 0·47 | 0·05 | 100·57 | 48·9 | 46·8 | 91·7 | 10·1 | Trans |
| 6K-458-3 | 3C | 13 | 51·43 | 1·36 | 0·24 | 0·08 | 7·09 | 1·05 | 1·11 | 0·21 | 3·21 | 1·54 | 0·10 | 0·03 | 17·30 | 5·37 | 19·68 | 7·70 | 0·44 | 0·16 | 100·60 | 42·6 | 52·0 | 90·6 | 9·5 | Dep |
| 6K-458-3 | 3R | 8 | 52·78 | 0·38 | 0·45 | 0·05 | 3·77 | 0·42 | 0·93 | 0·08 | 2·22 | 0·07 | 0·07 | 0·01 | 16·34 | 0·42 | 23·76 | 0·38 | 0·36 | 0·03 | 100·67 | 49·3 | 47·1 | 92·9 | 14·2 | Dep |
| 6K-458-3 | 4C | 9 | 51·41 | 0·68 | 0·20 | 0·05 | 6·48 | 0·17 | 1·04 | 0·06 | 3·57 | 0·87 | 0·11 | 0·02 | 18·22 | 3·15 | 18·06 | 4·09 | 0·42 | 0·14 | 99·50 | 39·1 | 54·9 | 90·1 | 9·7 | Dep |
| 6K-458-3 | 4R | 8 | 50·96 | 0·62 | 0·27 | 0·04 | 6·20 | 0·55 | 1·05 | 0·03 | 2·36 | 0·18 | 0·07 | 0·01 | 15·58 | 0·86 | 22·51 | 0·93 | 0·54 | 0·18 | 99·55 | 48·9 | 47·1 | 92·2 | 10·2 | Dep |
| 6K-458-3 | 5I | 11 | 51·69 | 0·43 | 0·32 | 0·04 | 5·22 | 0·42 | 0·92 | 0·06 | 2·24 | 0·12 | 0·06 | 0·02 | 15·47 | 0·42 | 23·07 | 0·31 | 0·44 | 0·05 | 99·42 | 49·8 | 46·4 | 92·5 | 10·6 | Dep |
| 6K-458-3 | 6I | 10 | 51·96 | 0·31 | 0·43 | 0·02 | 4·50 | 0·66 | 1·03 | 0·03 | 2·21 | 0·09 | 0·10 | 0·01 | 15·49 | 0·42 | 23·29 | 0·26 | 0·47 | 0·06 | 99·46 | 50·0 | 46·3 | 92·6 | 13·3 | Trans |
| 6K-465-2 | 1C | 8 | 50·64 | 0·59 | 0·23 | 0·04 | 6·24 | 0·06 | 1·10 | 0·05 | 3·13 | 0·68 | 0·11 | 0·02 | 17·38 | 2·89 | 20·57 | 3·81 | 0·30 | 0·09 | 99·69 | 43·6 | 51·2 | 90·8 | 10·5 | Dep |
| 6K-465-2 | 1R | 13 | 51·99 | 0·56 | 0·30 | 0·02 | 3·66 | 0·38 | 1·28 | 0·05 | 2·49 | 0·17 | 0·05 | 0·02 | 16·64 | 0·51 | 23·02 | 0·81 | 0·26 | 0·05 | 99·71 | 47·9 | 48·1 | 92·2 | 19·0 | Dep |
| 6K-465-2 | 2C | 10 | 51·18 | 0·39 | 0·21 | 0·03 | 6·45 | 0·06 | 1·09 | 0·04 | 3·25 | 0·55 | 0·03 | 0·03 | 17·10 | 2·25 | 20·63 | 3·06 | 0·30 | 0·06 | 100·23 | 43·9 | 50·7 | 90·4 | 10·2 | Dep |
| 6K-465-2 | 2R | 10 | 51·72 | 0·52 | 0·24 | 0·03 | 5·57 | 0·42 | 0·96 | 0·06 | 3·07 | 0·47 | 0·04 | 0·02 | 17·05 | 1·83 | 21·50 | 2·58 | 0·31 | 0·06 | 100·46 | 45·2 | 49·8 | 90·8 | 10·4 | Dep |
| 6K-465-2 | 3C | 8 | 51·25 | 0·15 | 0·25 | 0·03 | 5·38 | 0·52 | 1·03 | 0·02 | 2·90 | 0·13 | 0·06 | 0·02 | 16·40 | 0·23 | 22·98 | 0·63 | 0·19 | 0·06 | 100·45 | 47·8 | 47·5 | 91·0 | 11·4 | Dep |
| 6K-465-2 | 3R | 8 | 51·33 | 0·48 | 0·33 | 0·02 | 4·75 | 0·21 | 1·11 | 0·03 | 2·81 | 0·18 | 0·07 | 0·02 | 16·59 | 0·63 | 22·95 | 0·89 | 0·22 | 0·05 | 100·16 | 47·6 | 47·9 | 91·3 | 13·5 | Dep |
| 6K-465-2 | 4C | 10 | 51·91 | 0·34 | 0·26 | 0·04 | 4·15 | 0·40 | 1·14 | 0·04 | 2·67 | 0·16 | 0·07 | 0·01 | 16·92 | 0·27 | 23·01 | 0·47 | 0·19 | 0·04 | 100·30 | 47·3 | 48·4 | 91·9 | 15·6 | Dep |
| 6K-465-2 | 4R | 10 | 51·60 | 0·65 | 0·30 | 0·03 | 4·40 | 0·51 | 1·14 | 0·03 | 2·80 | 0·12 | 0·06 | 0·02 | 16·62 | 0·54 | 22·90 | 0·70 | 0·18 | 0·05 | 99·99 | 47·5 | 48·0 | 91·4 | 14·8 | Dep |
| 6K-465-2 | 5C | 10 | 50·45 | 0·43 | 0·24 | 0·03 | 6·41 | 0·56 | 1·20 | 0·03 | 3·01 | 0·09 | 0·10 | 0·02 | 15·98 | 0·30 | 22·37 | 0·33 | 0·41 | 0·06 | 100·17 | 47·6 | 47·4 | 90·4 | 11·2 | Enr |
| 6K-465-2 | 6C | 9 | 51·38 | 0·54 | 0·18 | 0·04 | 6·04 | 0·34 | 1·06 | 0·04 | 3·78 | 0·45 | 0·11 | 0·01 | 19·24 | 2·14 | 18·03 | 2·79 | 0·39 | 0·05 | 100·20 | 37·8 | 56·1 | 90·1 | 10·5 | Trans |
| 6K-465-2 | 6R | 9 | 51·15 | 1·11 | 0·26 | 0·06 | 5·35 | 0·26 | 1·10 | 0·13 | 2·98 | 1·18 | 0·10 | 0·03 | 16·84 | 4·98 | 21·66 | 6·63 | 0·41 | 0·15 | 99·85 | 45·7 | 49·4 | 91·0 | 12·1 | Trans |
| 6K-465-2 | 8C | 15 | 51·34 | 0·49 | 0·20 | 0·02 | 6·46 | 0·16 | 1·15 | 0·03 | 3·51 | 0·15 | 0·10 | 0·01 | 18·15 | 0·43 | 19·43 | 0·45 | 0·38 | 0·05 | 100·72 | 41·0 | 53·2 | 90·2 | 10·7 | Dep |
| 6K-465-2 | 8R | 18 | 51·08 | 1·23 | 0·26 | 0·08 | 5·55 | 0·31 | 1·16 | 0·13 | 2·84 | 1·37 | 0·10 | 0·02 | 15·97 | 5·63 | 22·89 | 7·71 | 0·39 | 0·20 | 100·25 | 48·4 | 46·9 | 90·9 | 12·3 | Dep |
| 6K-465-2 | 9C | 8 | 52·59 | 0·57 | 0·25 | 0·03 | 3·23 | 0·52 | 1·26 | 0·03 | 2·56 | 0·08 | 0·10 | 0·02 | 17·01 | 0·49 | 23·08 | 0·24 | 0·42 | 0·05 | 100·51 | 47·4 | 48·5 | 92·2 | 20·8 | Enr |
| 6K-465-2 | 9R | 10 | 52·37 | 0·75 | 0·31 | 0·05 | 3·52 | 0·85 | 1·20 | 0·11 | 2·55 | 0·07 | 0·11 | 0·02 | 16·82 | 0·39 | 23·04 | 0·43 | 0·40 | 0·05 | 100·29 | 47·6 | 48·3 | 92·2 | 18·6 | Enr |
| 6K-466-1 | 1C | 10 | 51·97 | 0·29 | 0·26 | 0·02 | 5·55 | 0·10 | 1·16 | 0·03 | 2·51 | 0·34 | 0·04 | 0·02 | 16·42 | 1·16 | 21·88 | 1·49 | 0·64 | 0·05 | 100·44 | 46·9 | 48·9 | 92·1 | 12·2 | |
| 6K-466-1 | 1R | 10 | 51·94 | 0·29 | 0·29 | 0·02 | 5·34 | 0·33 | 1·19 | 0·06 | 2·14 | 0·06 | 0·04 | 0·02 | 15·89 | 0·22 | 23·21 | 0·22 | 0·58 | 0·05 | 100·64 | 49·4 | 47·0 | 93·0 | 13·0 | |
| 6K-466-1 | 3I | 13 | 52·16 | 0·93 | 0·25 | 0·06 | 5·18 | 0·36 | 1·02 | 0·18 | 2·98 | 1·05 | 0·13 | 0·03 | 17·90 | 4·56 | 19·72 | 5·84 | 0·70 | 0·14 | 100·05 | 42·0 | 53·0 | 91·5 | 11·7 | |
| 6K-643-13 | 1I | 8 | 51·78 | 0·30 | 0·15 | 0·02 | 5·14 | 0·15 | 1·05 | 0·04 | 2·79 | 0·20 | 0·10 | 0·02 | 17·03 | 0·47 | 21·90 | 0·63 | 0·27 | 0·04 | 100·20 | 45·8 | 49·6 | 91·6 | 12·0 | |
| 6K-643-13 | 2C | 10 | 51·39 | 0·94 | 0·13 | 0·04 | 6·15 | 0·22 | 1·28 | 0·12 | 4·03 | 1·12 | 0·12 | 0·02 | 20·10 | 4·98 | 16·47 | 6·97 | 0·18 | 0·09 | 99·84 | 34·6 | 58·8 | 89·9 | 12·2 | |
| 6K-643-13 | 2R | 10 | 51·43 | 0·43 | 0·14 | 0·02 | 5·76 | 0·07 | 1·21 | 0·03 | 3·11 | 0·35 | 0·11 | 0·02 | 17·47 | 1·62 | 20·44 | 2·17 | 0·23 | 0·04 | 99·90 | 43·3 | 51·5 | 90·9 | 12·4 | |
| JR31-52-3 | 4C | 12 | 51·13 | 0·31 | 0·18 | 0·02 | 6·46 | 0·10 | 1·25 | 0·04 | 2·66 | 0·22 | 0·08 | 0·01 | 16·12 | 0·80 | 21·46 | 0·88 | 0·61 | 0·05 | 99·95 | 46·7 | 48·8 | 91·5 | 11·5 | |
| JR31-52-3 | 4R | 10 | 51·25 | 0·32 | 0·18 | 0·01 | 6·25 | 0·08 | 1·20 | 0·05 | 2·60 | 0·13 | 0·08 | 0·02 | 16·40 | 0·63 | 21·27 | 0·74 | 0·60 | 0·03 | 99·82 | 46·1 | 49·5 | 91·8 | 11·4 | |
| JR31-52-3 | 5C | 12 | 51·73 | 0·59 | 0·15 | 0·04 | 6·53 | 0·16 | 1·20 | 0·11 | 3·69 | 1·06 | 0·09 | 0·02 | 19·35 | 3·94 | 16·93 | 5·34 | 0·47 | 0·18 | 100·12 | 36·2 | 57·6 | 90·3 | 11·0 | |
| JR31-52-3 | 5R | 12 | 50·81 | 0·39 | 0·19 | 0·02 | 6·65 | 0·10 | 1·30 | 0·04 | 2·60 | 0·20 | 0·07 | 0·03 | 15·97 | 0·77 | 21·54 | 1·02 | 0·59 | 0·05 | 99·72 | 47·0 | 48·5 | 91·6 | 11·6 | |
| JR31-52-3 | 6I | 12 | 51·21 | 0·21 | 0·20 | 0·02 | 6·54 | 0·06 | 1·27 | 0·04 | 2·63 | 0·13 | 0·08 | 0·03 | 15·75 | 0·39 | 21·66 | 0·51 | 0·58 | 0·05 | 99·93 | 47·5 | 48·0 | 91·4 | 11·5 | |
| JR31-52-3 | 7C | 11 | 51·30 | 0·49 | 0·18 | 0·01 | 6·06 | 0·08 | 1·22 | 0·02 | 2·62 | 0·19 | 0·12 | 0·02 | 16·27 | 0·76 | 21·20 | 0·98 | 0·60 | 0·04 | 99·59 | 46·2 | 49·3 | 91·7 | 11·9 | |
| JR31-52-3 | 7R | 10 | 51·57 | 0·39 | 0·19 | 0·02 | 5·43 | 0·26 | 1·02 | 0·06 | 2·41 | 0·17 | 0·09 | 0·02 | 16·47 | 0·34 | 21·88 | 0·46 | 0·56 | 0·05 | 99·62 | 46·9 | 49·1 | 92·4 | 11·2 | |
| JR31-52-3 | 8I | 9 | 51·81 | 0·34 | 0·18 | 0·03 | 5·56 | 0·10 | 1·07 | 0·04 | 2·65 | 0·36 | 0·09 | 0·02 | 16·94 | 1·23 | 21·14 | 1·66 | 0·58 | 0·05 | 100·04 | 45·2 | 50·4 | 91·9 | 11·4 | |
| JR31-52-3 | 9I | 11 | 51·10 | 0·27 | 0·20 | 0·02 | 5·80 | 0·11 | 1·08 | 0·03 | 2·57 | 0·14 | 0·07 | 0·03 | 16·62 | 0·47 | 21·25 | 0·69 | 0·61 | 0·02 | 99·31 | 45·8 | 49·8 | 92·0 | 11·1 | |
| JR31-52-4 | 4C | 11 | 51·82 | 0·20 | 0·21 | 0·02 | 5·96 | 0·25 | 1·21 | 0·05 | 2·23 | 0·11 | 0·07 | 0·02 | 15·49 | 0·13 | 22·28 | 0·17 | 0·63 | 0·04 | 99·89 | 48·9 | 47·3 | 92·5 | 12·0 | |
| JR31-52-4 | 4R | 11 | 51·84 | 0·32 | 0·23 | 0·03 | 5·75 | 0·52 | 1·15 | 0·10 | 2·32 | 0·08 | 0·07 | 0·01 | 15·47 | 0·22 | 22·55 | 0·19 | 0·55 | 0·04 | 99·92 | 49·2 | 46·9 | 92·2 | 11·8 | |
| JR31-52-5 | 1C | 10 | 51·62 | 1·14 | 0·17 | 0·06 | 6·62 | 0·28 | 1·21 | 0·16 | 3·15 | 1·68 | 0·11 | 0·03 | 18·01 | 6·21 | 18·67 | 8·30 | 0·49 | 0·22 | 100·05 | 40·4 | 54·2 | 91·1 | 10·9 | |
| JR31-52-5 | 1R | 10 | 52·19 | 0·29 | 0·21 | 0·02 | 5·28 | 0·54 | 0·96 | 0·08 | 2·19 | 0·08 | 0·09 | 0·02 | 15·75 | 0·46 | 23·15 | 0·27 | 0·42 | 0·07 | 100·23 | 49·5 | 46·8 | 92·8 | 10·8 | |
| JR31-52-5 | 3C | 9 | 51·79 | 0·36 | 0·19 | 0·02 | 5·68 | 0·22 | 1·03 | 0·05 | 2·28 | 0·14 | 0·09 | 0·01 | 16·33 | 0·62 | 22·06 | 0·60 | 0·55 | 0·06 | 100·00 | 47·4 | 48·8 | 92·7 | 10·9 | |
| JR31-52-5 | 5I | 11 | 51·78 | 0·34 | 0·18 | 0·02 | 5·98 | 0·18 | 1·04 | 0·04 | 2·64 | 0·26 | 0·04 | 0·02 | 16·31 | 1·07 | 21·46 | 1·25 | 0·56 | 0·04 | 99·99 | 46·4 | 49·1 | 91·7 | 10·5 | |
| JR31-52-5 | 6I | 8 | 51·57 | 0·37 | 0·22 | 0·03 | 5·96 | 0·09 | 1·09 | 0·03 | 2·51 | 0·06 | 0·04 | 0·03 | 15·86 | 0·22 | 22·06 | 0·35 | 0·56 | 0·04 | 99·86 | 47·9 | 47·9 | 91·8 | 11·0 | |

(continued)

*Table 3: Continued*

| Analysis | Grn* | Pts | SiO$_2$ | ± | TiO$_2$ | ± | Al$_2$O$_3$ | ± | Cr$_2$O$_3$ | ± | FeO | ± | MnO | ± | MgO | ± | CaO | ± | Na$_2$O | ± | Total | Wo | En | Mg-no. | Cr-no. | Notes† |
|---|---|---|---|---|---|---|---|---|---|---|---|---|---|---|---|---|---|---|---|---|---|---|---|---|---|---|
| JR31-52-8 | 1C | 10 | 51·18 | 0·28 | 0·18 | 0·02 | 6·21 | 0·11 | 1·22 | 0·05 | 2·77 | 0·38 | 0·12 | 0·02 | 16·38 | 1·37 | 20·87 | 1·92 | 0·56 | 0·08 | 99·49 | 45·6 | 49·7 | 91·3 | 11·6 | |
| JR31-52-8 | 1R | 20 | 51·55 | 0·45 | 0·21 | 0·03 | 6·06 | 0·38 | 1·16 | 0·10 | 2·60 | 0·45 | 0·10 | 0·02 | 16·39 | 1·09 | 21·21 | 1·71 | 0·57 | 0·07 | 99·85 | 46·1 | 49·5 | 91·8 | 11·4 | |
| JR31-52-8 | 3I | 9 | 51·71 | 0·15 | 0·18 | 0·01 | 5·64 | 0·10 | 1·11 | 0·04 | 2·62 | 0·27 | 0·08 | 0·02 | 16·17 | 0·98 | 21·21 | 1·35 | 0·66 | 0·07 | 99·38 | 46·4 | 49·2 | 91·7 | 11·7 | |
| JR31-52-8 | 4R | 9 | 51·91 | 0·25 | 0·22 | 0·02 | 5·43 | 0·28 | 1·01 | 0·10 | 2·46 | 0·08 | 0·09 | 0·02 | 16·19 | 0·35 | 21·80 | 0·40 | 0·62 | 0·06 | 99·74 | 47·1 | 48·7 | 92·1 | 11·1 | |
| RC27-9-6-5 | 1C | 8 | 51·00 | 1·13 | 0·16 | 0·08 | 6·75 | 0·16 | 1·08 | 0·16 | 3·96 | 1·95 | 0·12 | 0·03 | 19·09 | 6·28 | 16·99 | 8·82 | 0·46 | 0·17 | 99·60 | 36·4 | 56·9 | 89·6 | 9·7 | Enr |
| RC27-9-6-5 | 1R | 5 | 51·27 | 0·81 | 0·27 | 0·08 | 4·38 | 1·76 | 1·16 | 0·02 | 2·66 | 0·35 | 0·10 | 0·03 | 16·35 | 0·83 | 22·65 | 1·35 | 0·44 | 0·08 | 99·28 | 47·7 | 47·9 | 91·6 | 15·1 | Enr |
| RC27-9-6-5 | 2C | 8 | 51·26 | 1·08 | 0·17 | 0·07 | 6·67 | 0·19 | 1·14 | 0·13 | 3·71 | 1·63 | 0·11 | 0·04 | 18·34 | 5·21 | 18·74 | 7·56 | 0·36 | 0·15 | 100·51 | 39·7 | 54·1 | 89·8 | 10·3 | Trans |
| RC27-9-6-5 | 2R | 9 | 51·44 | 0·71 | 0·49 | 0·13 | 5·65 | 0·35 | 1·09 | 0·04 | 3·14 | 0·36 | 0·09 | 0·02 | 17·15 | 1·22 | 21·39 | 1·54 | 0·42 | 0·06 | 100·86 | 44·8 | 50·0 | 90·7 | 11·5 | Trans |
| RC27-9-6-5 | 3I | 6 | 52·40 | 0·80 | 0·49 | 0·19 | 2·50 | 0·80 | 0·96 | 0·33 | 2·23 | 0·12 | 0·08 | 0·02 | 17·19 | 0·60 | 23·37 | 0·52 | 0·45 | 0·16 | 99·68 | 47·7 | 48·8 | 93·2 | 20·5 | Enr |
| RC27-9-6-5 | 4C | 13 | 51·57 | 0·25 | 0·31 | 0·04 | 5·73 | 0·11 | 1·08 | 0·03 | 3·04 | 0·45 | 0·04 | 0·02 | 16·25 | 1·31 | 21·76 | 1·89 | 0·50 | 0·05 | 100·28 | 46·6 | 48·4 | 90·5 | 11·2 | Enr |
| RC27-9-6-5 | 4R | 10 | 52·24 | 0·71 | 0·47 | 0·05 | 3·61 | 0·89 | 0·98 | 0·09 | 2·80 | 0·29 | 0·10 | 0·01 | 16·41 | 0·82 | 22·22 | 0·87 | 0·39 | 0·06 | 99·23 | 47·0 | 48·3 | 91·3 | 15·3 | Enr |
| RC27-9-6-5 | 5C | 8 | 51·76 | 1·33 | 0·34 | 0·11 | 5·79 | 0·57 | 1·07 | 0·15 | 3·91 | 1·75 | 0·11 | 0·04 | 19·36 | 5·68 | 17·42 | 7·94 | 0·60 | 0·27 | 100·35 | 36·8 | 56·8 | 89·8 | 11·0 | Enr |
| RC27-9-6-5 | 5R | 11 | 52·45 | 1·08 | 0·55 | 0·15 | 3·87 | 0·84 | 1·19 | 0·20 | 2·58 | 0·49 | 0·04 | 0·03 | 17·39 | 2·14 | 21·28 | 2·57 | 0·71 | 0·25 | 100·06 | 44·8 | 50·9 | 92·3 | 17·1 | Enr |
| RC27-9-6-5 | L11C | 10 | 51·3 | 0·6 | 0·24 | 0·03 | 6·23 | 1·06 | 1·13 | 0·08 | 3·11 | 0·29 | 0·09 | 0·02 | 16·30 | 0·87 | 22·06 | 1·67 | 0·39 | 0·23 | 100·85 | 46·8 | 48·1 | 90·3 | 10·8 | |
| RC27-9-6-5 | L11R | 10 | 51·8 | 0·6 | 0·25 | 0·03 | 5·55 | 0·89 | 0·88 | 0·08 | 2·82 | 0·44 | 0·07 | 0·02 | 16·46 | 1·10 | 22·64 | 1·73 | 0·35 | 0·10 | 100·82 | 47·4 | 48·0 | 91·2 | 9·6 | |
| RC27-9-6-7 | 1C | 10 | 51·59 | 1·43 | 0·16 | 0·09 | 6·33 | 0·27 | 1·07 | 0·18 | 4·21 | 2·05 | 0·14 | 0·02 | 20·46 | 7·42 | 15·56 | 10·04 | 0·33 | 0·23 | 99·85 | 32·9 | 60·2 | 89·6 | 10·2 | |
| RC27-9-6-7 | 1R | 10 | 51·34 | 0·95 | 0·22 | 0·05 | 5·86 | 0·53 | 1·02 | 0·14 | 3·05 | 0·93 | 0·11 | 0·02 | 16·88 | 3·37 | 21·22 | 4·40 | 0·35 | 0·09 | 100·05 | 45·1 | 49·9 | 90·8 | 10·5 | |
| RC27-9-6-7 | 3I | 10 | 51·49 | 0·38 | 0·23 | 0·03 | 5·76 | 0·12 | 0·93 | 0·06 | 3·09 | 0·56 | 0·08 | 0·02 | 17·04 | 2·04 | 21·26 | 2·57 | 0·39 | 0·09 | 100·27 | 44·9 | 50·0 | 90·8 | 9·8 | |
| RC27-9-6-7 | 5I | 7 | 50·83 | 0·99 | 0·25 | 0·04 | 5·50 | 0·93 | 0·92 | 0·17 | 2·78 | 0·22 | 0·09 | 0·02 | 16·39 | 0·55 | 22·59 | 1·03 | 0·41 | 0·09 | 99·78 | 47·5 | 47·9 | 91·3 | 10·1 | |

*Grain number and core (C), rim (R) or interstitial (I). Interstitial grains are <1 mm diameter. L preceding a grain number indicates Lee (1997) data for dredge RC27-9-6 samples.
†Dep, Trans and Enr refer to depleted, transitional and enriched zones of the cryptically metasomatized samples.

(Figs 2 and 3; Table 2). In hand specimen and thin section, all 14 peridotites look like 'typical' abyssal peridotites, with either porphyroclastic or protogranular textures and variable degrees of alteration (Figs 2 and 3). None of the peridotites contain veins. The modal variation of the peridotites is shown in Fig. 4, with Cpx modes varying by 3–9%, within the range of previously published modes for Atlantis II peridotites (Johnson & Dick, 1992; Kumagai *et al.*, 2003; Morishita *et al.*, 2007). All of these observations suggest that the peridotites are the depleted residues of melt extraction, and the REE concentrations in 10 of the samples agree with this interpretation. As shown in Fig. 5, these 10 residual peridotites have depleted REE patterns and are within the range of previously measured Atlantis II Fracture Zone peridotites.

The remaining four peridotites in this study have a large range in cpx trace element concentrations (6K-458-3, 6K-465-2, and RC27-9-6-5) or an enriched composition (6K-458-1), as shown in Fig. 6. On the basis of the trace element enrichment, these peridotites are classified as cryptically metasomatized. In three of the four peridotites, 1–3 orders of magnitude variation in trace element concentration occurs across <2 cm distance. In one Cpx porphyroclast (Fig. 3c), Ce concentrations vary from 0·1 to 2 ppm over a distance of <2 mm.

In hand specimen and thin section, the cryptically metasomatized peridotites have no veins and look like the other peridotites. Among the cryptically metasomatized peridotites, 6K-465-2 and RC27-9-6-5 have <50% alteration, with all primary phases present. The two samples from dive 6K-458 are more altered, with >50% serpentinization and no olivine preserved in 6K-458-3. Figure 2 shows the hand specimen for sample 6K-465-2, which has a modal composition similar to that of the other peridotites in this study (Fig. 4). This sample contains none of the talc and amphibole veins that are found in some peridotites and that are often interpreted as altered melt veins. The edges of 6K-465-2 are planar, which could be interpreted as the contact with a vein. However, there is no alteration halo at the edge of the sample, as is often found at vein contacts. In addition, sample RC27-9-6-5, which also exhibits a large range in trace elements, is sub-angular in shape with no planar surfaces that would represent a likely vein contact. This sample does contain a ∼1 mm wide zone of recrystallized olivine that is close to the zone of observed trace element enrichment. The role of melt–rock reaction in enhancing deformation in peridotites has been discussed elsewhere (e.g. Dijkstra *et al.*, 2002) and was not pursued further in this study, particularly as the

*Table 4: Major element compositions of Opx (in wt %)*

| Analysis | Grn* | Pts | $SiO_2$ | ± | $TiO_2$ | ± | $Al_2O_3$ | ± | $Cr_2O_3$ | ± | FeO | ± | MnO | ± | MgO | ± | CaO | ± | $Na_2O$ | ± | Total | Wo | En | Mg-no. | Cr-no. | Notes† |
|---|---|---|---|---|---|---|---|---|---|---|---|---|---|---|---|---|---|---|---|---|---|---|---|---|---|---|
| 6K-458-1 | 1C | 8 | 53·01 | 1·81 | 0·10 | 0·04 | 4·17 | 0·89 | 1·38 | 0·81 | 6·43 | 1·08 | 0·21 | 0·07 | 32·27 | 1·15 | 1·24 | 1·26 | 0·07 | 0·07 | 98·88 | 2·4 | 87·8 | 89·9 | 18·1 | Enr |
| 6K-458-1 | 1R | 8 | 54·82 | 0·44 | 0·09 | 0·02 | 5·05 | 0·14 | 0·85 | 0·03 | 6·05 | 0·15 | 0·14 | 0·01 | 32·43 | 0·51 | 1·29 | 0·71 | 0·02 | 0·02 | 100·74 | 2·5 | 88·2 | 90·5 | 10·2 | Enr |
| 6K-458-3 | 1C | 13 | 54·17 | 0·29 | 0·09 | 0·03 | 5·64 | 0·24 | 0·75 | 0·03 | 6·12 | 0·23 | 0·12 | 0·02 | 30·56 | 0·88 | 1·97 | 1·04 | 0·01 | 0·01 | 99·42 | 4·0 | 86·3 | 89·9 | 8·2 | Dep |
| 6K-458-3 | 1C | 9 | 54·77 | 0·24 | 0·08 | 0·02 | 4·91 | 0·11 | 0·62 | 0·02 | 6·23 | 0·16 | 0·12 | 0·03 | 31·18 | 0·46 | 1·32 | 0·65 | 0·00 | 0·00 | 99·24 | 2·7 | 87·5 | 89·9 | 7·8 | Dep |
| 6K-465-2 | 1C | 10 | 55·44 | 0·29 | 0·09 | 0·01 | 4·17 | 0·16 | 0·64 | 0·01 | 6·32 | 0·12 | 0·12 | 0·01 | 32·18 | 0·37 | 1·58 | 0·41 | 0·03 | 0·01 | 100·57 | 3·1 | 87·3 | 90·1 | 9·3 | Dep |
| 6K-465-2 | 1R | 10 | 55·78 | 0·34 | 0·09 | 0·01 | 3·34 | 0·46 | 0·61 | 0·02 | 6·35 | 0·10 | 0·12 | 0·02 | 33·04 | 0·45 | 1·19 | 0·20 | 0·03 | 0·01 | 100·54 | 2·3 | 88·2 | 90·3 | 10·9 | Dep |
| 6K-465-2 | 2C | 3 | 53·42 | 0·30 | 0·07 | 0·02 | 5·51 | 0·21 | 0·81 | 0·05 | 6·12 | 0·29 | 0·13 | 0·03 | 31·24 | 0·53 | 1·77 | 0·84 | 0·00 | 0·00 | 99·07 | 3·5 | 86·9 | 90·1 | 9·0 | Dep |
| 6K-466-1 | 1C | 10 | 54·70 | 0·50 | 0·08 | 0·03 | 4·57 | 0·15 | 0·77 | 0·03 | 5·80 | 0·29 | 0·14 | 0·05 | 31·80 | 0·91 | 2·37 | 1·22 | 0·04 | 0·04 | 100·27 | 4·6 | 86·5 | 90·7 | 10·2 | |
| 6K-466-1 | 1R | 10 | 55·77 | 0·30 | 0·07 | 0·01 | 3·98 | 0·07 | 0·60 | 0·03 | 5·92 | 0·15 | 0·14 | 0·02 | 32·74 | 0·45 | 1·36 | 0·45 | 0·02 | 0·02 | 100·59 | 2·6 | 88·4 | 90·8 | 9·2 | |
| 6K-466-1 | 2I | 6 | 54·89 | 0·33 | 0·07 | 0·01 | 3·49 | 0·14 | 0·44 | 0·02 | 5·96 | 0·13 | 0·17 | 0·02 | 34·22 | 0·30 | 0·78 | 0·06 | | | 100·01 | 1·5 | 89·8 | 91·1 | 7·8 | |
| 6K-643-13 | 1C | 10 | 54·19 | 0·21 | 0·05 | 0·01 | 5·07 | 0·10 | 0·90 | 0·04 | 5·97 | 0·16 | 0·13 | 0·02 | 31·15 | 0·56 | 2·18 | 0·55 | 0·02 | 0·01 | 99·65 | 4·4 | 86·4 | 90·3 | 10·6 | |
| 6K-643-13 | 1R | 9 | 54·90 | 0·46 | 0·05 | 0·02 | 3·98 | 0·27 | 0·67 | 0·05 | 6·01 | 0·30 | 0·13 | 0·02 | 32·05 | 1·29 | 1·92 | 1·75 | 0·01 | 0·01 | 99·71 | 3·8 | 87·1 | 90·5 | 10·1 | |
| JR31-52-3 | 1C | 13 | 54·36 | 0·29 | 0·06 | 0·02 | 5·45 | 0·13 | 0·90 | 0·03 | 5·97 | 0·17 | 0·13 | 0·02 | 30·94 | 0·47 | 1·96 | 0·56 | 0·06 | 0·03 | 99·84 | 3·9 | 86·7 | 90·2 | 10·0 | |
| JR31-52-3 | 1R | 10 | 55·17 | 0·36 | 0·05 | 0·01 | 4·29 | 0·29 | 0·58 | 0·07 | 6·01 | 0·19 | 0·13 | 0·02 | 32·00 | 0·39 | 1·21 | 0·40 | 0·02 | 0·01 | 99·45 | 2·4 | 88·3 | 90·5 | 8·4 | |
| JR31-52-4 | 1C | 16 | 54·25 | 0·25 | 0·08 | 0·02 | 5·25 | 0·09 | 0·71 | 0·08 | 5·97 | 0·20 | 0·12 | 0·03 | 31·24 | 0·62 | 1·80 | 0·79 | 0·06 | 0·03 | 99·47 | 3·6 | 87·1 | 90·3 | 8·3 | |
| JR31-52-4 | 1R | 11 | 54·46 | 0·12 | 0·08 | 0·01 | 5·18 | 0·07 | 0·79 | 0·02 | 5·91 | 0·23 | 0·12 | 0·02 | 31·07 | 0·96 | 2·12 | 1·28 | 0·06 | 0·04 | 99·80 | 4·3 | 86·5 | 90·4 | 9·3 | |
| JR31-52-4 | 2I | 12 | 55·77 | 0·28 | 0·08 | 0·01 | 3·63 | 0·20 | 0·43 | 0·05 | 6·12 | 0·11 | 0·13 | 0·02 | 32·81 | 0·19 | 0·89 | 0·08 | 0·02 | 0·01 | 99·89 | 1·7 | 89·0 | 90·5 | 7·4 | |
| JR31-52-5 | 1C | 13 | 54·17 | 0·49 | 0·08 | 0·01 | 5·38 | 0·15 | 0·81 | 0·04 | 5·84 | 0·16 | 0·14 | 0·03 | 30·86 | 0·68 | 2·30 | 0·89 | 0·05 | 0·03 | 99·63 | 4·6 | 86·2 | 90·4 | 9·2 | |
| JR31-52-5 | 1R | 11 | 54·59 | 0·40 | 0·05 | 0·02 | 5·15 | 0·28 | 0·76 | 0·04 | 5·93 | 0·18 | 0·08 | 0·02 | 31·78 | 0·42 | 1·20 | 0·37 | 0·04 | 0·01 | 99·58 | 2·4 | 88·4 | 90·5 | 9·0 | |
| JR31-52-8 | 1C | 15 | 54·45 | 0·42 | 0·09 | 0·02 | 5·16 | 0·24 | 0·80 | 0·05 | 5·93 | 0·18 | 0·11 | 0·03 | 30·88 | 0·72 | 2·30 | 1·00 | 0·06 | 0·03 | 99·79 | 4·6 | 86·1 | 90·3 | 9·5 | |
| JR31-52-8 | 1R | 15 | 55·82 | 0·51 | 0·08 | 0·01 | 3·68 | 0·31 | 0·42 | 0·09 | 6·16 | 0·16 | 0·12 | 0·02 | 32·64 | 0·34 | 0·83 | 0·26 | 0·02 | 0·02 | 99·76 | 1·6 | 89·0 | 90·4 | 7·0 | |
| JR31-52-8 | 3I | 10 | 56·00 | 0·20 | 0·05 | 0·01 | 3·94 | 0·11 | 0·57 | 0·02 | 6·10 | 0·10 | 0·12 | 0·02 | 32·37 | 0·19 | 1·32 | 0·17 | 0·05 | 0·01 | 100·53 | 2·6 | 88·1 | 90·4 | 8·9 | |
| RC27-9-6-5 | 1C | 9 | 55·02 | 0·52 | 0·09 | 0·02 | 3·82 | 0·55 | 0·68 | 0·04 | 6·30 | 0·14 | 0·09 | 0·02 | 31·30 | 0·60 | 1·56 | 0·71 | 0·04 | 0·03 | 98·91 | 3·1 | 87·0 | 89·8 | 10·7 | Trans |
| RC27-9-6-5 | 1R | 10 | 56·31 | 0·45 | 0·13 | 0·02 | 2·40 | 0·19 | 0·61 | 0·03 | 6·54 | 0·15 | 0·10 | 0·02 | 32·63 | 0·36 | 0·88 | 0·36 | 0·06 | 0·08 | 99·66 | 1·7 | 88·4 | 89·9 | 14·5 | Trans |
| RC27-9-6-5 | 5I | 7 | 55·77 | 0·83 | 0·08 | 0·01 | 3·30 | 0·32 | 0·70 | 0·04 | 6·49 | 0·02 | 0·14 | 0·02 | 32·39 | 0·24 | 1·10 | 0·31 | 0·01 | 0·01 | 99·99 | 2·2 | 87·9 | 89·9 | 12·5 | Enr |
| RC27-9-6-5 | L1C | 10 | 53·9 | 0·3 | 0·09 | 0·03 | 5·71 | 0·13 | 0·76 | 0·04 | 6·59 | 0·50 | 0·11 | 0·02 | 31·11 | 1·5 | 2·29 | 2·1 | 0·02 | 0·02 | 100·58 | 4·5 | 85·3 | 89·4 | 8·2 | |
| RC27-9-6-7 | 1C | 10 | 54·16 | 0·27 | 0·08 | 0·02 | 5·25 | 0·40 | 0·72 | 0·04 | 6·16 | 0·16 | 0·14 | 0·02 | 31·13 | 0·65 | 1·86 | 0·58 | 0·01 | 0·02 | 99·53 | 3·7 | 86·7 | 90·0 | 8·5 | |
| RC27-9-6-7 | 1R | 10 | 55·13 | 0·27 | 0·06 | 0·01 | 4·22 | 0·15 | 0·38 | 0·02 | 6·46 | 0·12 | 0·14 | 0·02 | 32·88 | 0·27 | 0·59 | 0·11 | 0·00 | 0·01 | 99·84 | 1·1 | 89·0 | 90·1 | 5·7 | |

*Grain number and core (C), rim (R) or interstitial (I). Interstitial grains are <1mm diameter. L preceding a grain number indicates Lee (1997) data for dredge RC27-9-6 samples.

†Dep, Trans and Enr refer to depleted, transitional and enriched zones of the cryptically metasomatized samples.

*Table 5:* *Major element compositions of olivine (in wt %)*

| Sample | Grn* | Pts | SiO$_2$ | ± | FeO | ± | MnO | ± | MgO | ± | NiO | ± | Total | Mg-no. | Notes† |
|---|---|---|---|---|---|---|---|---|---|---|---|---|---|---|---|
| 6K-458-1 | 1 | 6 | 40·55 | 0·26 | 9·22 | 0·18 | 0·08 | 0·03 | 49·64 | 0·29 | 0·34 | 0·04 | 99·87 | 90·6 | Enr |
| 6K-465-2 | 1 | 6 | 40·53 | 0·28 | 9·63 | 0·11 | 0·14 | 0·02 | 50·00 | 0·36 | 0·32 | 0·03 | 100·68 | 90·3 | Dep |
| 6K-465-2 | 2 | 6 | 41·91 | 0·28 | 9·39 | 0·09 |  |  | 49·32 | 0·19 |  |  | 100·67 | 90·3 | Dep |
| JR31-52-3 | 1 | 7 | 40·10 | 0·08 | 9·45 | 0·12 | 0·14 | 0·02 | 49·48 | 0·26 | 0·40 | 0·03 | 99·61 | 90·3 | |
| JR31-52-5 | 1 | 6 | 40·47 | 0·12 | 9·43 | 0·15 | 0·16 | 0·02 | 49·06 | 0·09 | 0·35 | 0·03 | 99·51 | 90·3 | |
| JR31-52-8 | 1 | 6 | 40·22 | 0·09 | 9·59 | 0·24 | 0·14 | 0·02 | 49·04 | 0·14 | 0·37 | 0·02 | 99·38 | 90·1 | |
| RC27-9-6-5 | L1 | 6 | 40·50 | 0·02 | 10·32 | 0·07 | 0·11 | 0·01 | 49·43 | 0·07 | 0·35 | 0·02 | 100·76 | 89·5 | |
| RC27-9-6-5 | L2 | 6 | 40·70 | 0·30 | 9·85 | 0·11 | 0·11 | 0·02 | 49·98 | 0·31 | 0·39 | 0·02 | 101·12 | 90·0 | |
| RC27-9-6-5 | 1 | 5 | 40·76 | 0·17 | 9·93 | 0·26 | 0·13 | 0·04 | 49·16 | 0·31 | 0·34 | 0·03 | 100·36 | 89·8 | Enr |
| RC27-9-6-7 | 1 | 6 | 41·08 | 0·18 | 9·60 | 0·06 | 0·14 | 0·01 | 49·33 | 0·61 | 0·31 | 0·02 | 100·50 | 90·2 | |

*Grain number; L preceding a grain number indicates Lee (1997) data for dredge RC27-9-6 samples.
†Dep and Enr refer to depleted and enriched zones of the cryptically metasomatized samples.

*Table 6:* *Major element compositions of spinel (in wt %)*

| Sample | Grn* | Pts | TiO$_2$ | ± | Al$_2$O$_3$ | ± | Cr$_2$O$_3$ | ± | Fe$_2$O$_3$ | ± | FeO | ± | MnO | ± | MgO | ± | NiO | ± | ZnO | ± | Total | Mg-no. | Cr-no. | Notes† |
|---|---|---|---|---|---|---|---|---|---|---|---|---|---|---|---|---|---|---|---|---|---|---|---|---|
| 6K-458-1 | 1 | 5 | 0·07 | 0·06 | 48·28 | 1·62 | 21·93 | 1·91 | 0·30 | 0·27 | 11·30 | 0·31 | 0·12 | 0·04 | 18·49 | 0·33 | 0·27 | 0·04 | 0·00 | 0·00 | 100·80 | 74·5 | 23·4 | Enr |
| 6K-458-3 | 1 | 6 | 0·05 | 0·01 | 55·41 | 0·41 | 14·72 | 0·52 | 0·00 | 0·00 | 11·33 | 0·15 | 0·15 | 0·03 | 18·90 | 0·19 | 0·32 | 0·02 | 0·12 | 0·04 | 101·06 | 74·8 | 15·1 | Dep |
| 6K-465-2 | 1 | 6 | 0·17 | 0·01 | 46·54 | 0·27 | 20·02 | 0·22 | 4·06 | 0·58 | 9·34 | 0·56 | 0·08 | 0·02 | 19·50 | 0·32 | 0·27 | 0·02 |  |  | 99·99 | 78·8 | 22·4 | Dep |
| 6K-465-2 | 2 | 6 | 0·29 | 0·02 | 28·89 | 1·05 | 37·78 | 0·59 | 2·55 | 0·56 | 16·49 | 0·49 | 0·25 | 0·04 | 12·89 | 0·17 | 0·11 | 0·03 |  |  | 99·34 | 58·2 | 46·7 | Dep |
| 6K-465-2 | 3 | 6 | 0·26 | 0·03 | 39·47 | 1·12 | 28·23 | 1·18 | 1·58 | 0·33 | 13·18 | 0·26 | 0·17 | 0·02 | 16·16 | 0·26 | 0·18 | 0·02 |  |  | 99·25 | 68·6 | 32·4 | Dep |
| 6K-466-1 | 1 | 6 | 0·10 | 0·02 | 48·21 | 0·16 | 19·61 | 0·16 | 2·97 | 0·31 | 8·47 | 0·15 | 0·09 | 0·02 | 20·17 | 0·14 | 0·29 | 0·02 |  |  | 99·92 | 80·9 | 21·4 | |
| 6K-643-13 | 1 | 4 | 0·02 | 0·03 | 47·53 | 0·31 | 20·85 | 0·14 | 1·18 | 0·19 | 10·78 | 0·14 | 0·11 | 0·03 | 18·36 | 0·03 | 0·33 | 0·01 | 0·00 | 0·00 | 99·17 | 75·2 | 22·7 | |
| JR31-52-3 | 1 | 6 | 0·02 | 0·02 | 53·01 | 0·44 | 16·48 | 0·27 | 0·36 | 0·31 | 11·03 | 0·29 | 0·15 | 0·03 | 19·01 | 0·13 | 0·31 | 0·03 |  |  | 100·37 | 75·4 | 17·3 | |
| JR31-52-4 | 2 | 6 | 0·09 | 0·11 | 52·57 | 0·18 | 16·07 | 0·31 | 0·00 | 0·00 | 12·13 | 0·26 | 0·12 | 0·03 | 18·08 | 0·14 | 0·28 | 0·03 |  |  | 99·37 | 72·6 | 17·0 | |
| JR31-52-5 | 1 | 6 | 0·04 | 0·01 | 51·41 | 1·23 | 17·53 | 1·09 | 0·86 | 0·50 | 10·90 | 0·39 | 0·13 | 0·01 | 18·90 | 0·25 | 0·30 | 0·03 |  |  | 100·09 | 75·5 | 18·6 | |
| JR31-52-8 | 1 | 6 | 0·07 | 0·02 | 52·46 | 0·17 | 16·73 | 0·18 | 0·19 | 0·20 | 11·07 | 0·36 | 0·11 | 0·03 | 18·86 | 0·15 | 0·31 | 0·03 |  |  | 99·81 | 75·2 | 17·6 | |
| RC27-9-6-5 | 1 | 6 | 0·21 | 0·03 | 42·99 | 3·91 | 24·44 | 3·71 | 2·07 | 0·66 | 13·16 | 0·96 | 0·17 | 0·05 | 16·57 | 0·96 | 0·30 | 0·03 | 0·18 | 0·07 | 100·12 | 69·2 | 27·6 | Dep |
| RC27-9-6-5 | 2 | 6 | 0·17 | 0·03 | 27·59 | 1·14 | 39·19 | 0·61 | 2·71 | 0·39 | 17·01 | 0·30 | 0·23 | 0·03 | 12·43 | 0·28 | 0·19 | 0·03 | 0·05 | 0·10 | 99·66 | 56·6 | 48·8 | Dep |
| RC27-9-6-5 | L1 | 6 | 0·32 | 0·09 | 46·56 | 2·30 | 20·61 | 2·26 | 2·43 |  | 11·63 | 0·60 | 0·25 | 0·02 | 17·87 | 0·44 | 0·41 | 0·03 |  |  | 100·14 | 73·3 | 22·9 | |
| RC27-9-6-7 | 1 | 3 | 0·00 | 0·01 | 49·49 | 2·90 | 15·73 | 0·46 | 3·74 | 2·34 | 11·29 | 1·03 | 0·24 | 0·26 | 18·12 | 1·03 | 0·33 | 0·03 | 0·00 | 0·00 | 99·03 | 74·1 | 17·6 | |
| RC27-9-6-7 | 2 | 6 | 0·00 | 0·00 | 51·79 | 0·76 | 15·58 | 0·57 | 1·67 | 0·44 | 11·95 | 0·31 | 0·07 | 0·03 | 18·15 | 0·38 | 0·31 | 0·02 | 0·00 | 0·00 | 99·57 | 73·0 | 16·8 | |

*Grain number; L preceding a grain number indicates Lee (1997) data for dredge RC27-9-6 samples.
†Dep and Enr refer to depleted and enriched zones of the cryptically metasomatized samples.

*Table 7:* *Major element compositions of plagioclase (in wt %)*

| Sample | Grn* | Pts | SiO$_2$ | ± | Al$_2$O$_3$ | ± | FeO | ± | CaO | ± | Na$_2$O | ± | Total | An |
|---|---|---|---|---|---|---|---|---|---|---|---|---|---|---|
| 6K-465-2 | 1 | 6 | 45·34 | 0·32 | 35·20 | 0·38 | 0·11 | 0·02 | 18·00 | 0·35 | 1·02 | 0·19 | 99·72 | 90·7 |
| 6K-465-2 | 2 | 6 | 44·75 | 0·14 | 35·35 | 0·15 | 0·13 | 0·04 | 18·42 | 0·11 | 0·74 | 0·04 | 99·44 | 93·2 |
| 6K-465-2 | 3 | 7 | 45·29 | 0·36 | 35·02 | 0·35 | 0·15 | 0·04 | 18·04 | 0·21 | 1·06 | 0·07 | 99·60 | 90·4 |
| RC27-9-6-5 | L1 | 6 | 47·2 | 0·4 | 33·62 | 0·28 | 0·10 | 0·03 | 17·02 | 0·18 | 1·84 | 0·19 | 101·03 | 83·6 |
| RC27-9-6-5 | 1 | 6 | 47·19 | 0·32 | 34·64 | 0·40 | 0·11 | 0·04 | 16·75 | 0·30 | 1·74 | 0·21 | 100·44 | 84·1 |

*All grains are interstitial and from the depleted zones of cryptically metasomatized peridotites. L preceding a grain number indicates Lee (1997) data for dredge RC27-9-6 samples.

*Table 8: Ion probe trace element concentrations (in ppm) for cryptically metasomatized peridotite Cpx*

| Sample | Grain | Type[a] | La | Ce | Nd | Sm | Eu | Dy | Er | Yb | Na$_2$O | Ti | Cr | Sr | Y | Zr | Notes† |
|---|---|---|---|---|---|---|---|---|---|---|---|---|---|---|---|---|---|
| KH1‡ | Cpx | | 1·220 | 5·39 | 5·56 | 2·12 | 0·75 | 2·30 | 1·12 | 0·99 | | | | | | | |
| KL2G§ | Basalt | | | | | | | | | | 2·27 | 15200 | 290 | 362·00 | 27 | 160·00 | |
| KLB1, av., n = 21 | Cpx | | 0·223 | 1·86 | 3·29 | 1·70 | 0·70 | 2·83 | 1·67 | 1·49 | | | | | | | |
| KLB1, SD | Cpx | | 0·038 | 0·21 | 0·38 | 0·25 | 0·07 | 0·25 | 0·18 | 0·18 | | | | | | | |
| KLB1, error (%) | Cpx | | 17 | 11 | 11 | 15 | 10 | 8·9 | 11 | 12 | | | | | | | |
| Count error (%) | Cpx | | 21 | 13 | 10 | 10 | 8·2 | 4·9 | 6·2 | 5·5 | 0·3 | 0·6 | 0·2 | 5·9 | 2·2 | 7·0 | |
| Duplicate error (%)** | Cpx | | 32 | 37 | 16 | 17 | 17 | 15 | 18 | 19 | 7·6 | 11 | 6·8 | 14 | 9·4 | 17 | |
| 6K-458-1 | Cpx1 | Core | 0·588 | 1·86 | 1·51 | 1·28 | 0·38 | 2·18 | 1·24 | 1·21 | 0·56 | 1470 | 7430 | 3·05 | 18·36 | 5·39 | Enr |
| 6K-458-1 | Cpx1 | Rim | 0·725 | 3·55 | 3·35 | 1·78 | 0·47 | 3·83 | 2·16 | 1·85 | 0·48 | 2122 | 8246 | 1·72 | 22·13 | 23·22 | Enr |
| 6K-458-1 | Cpx2 | Ints | 0·658 | 3·33 | 3·22 | 1·95 | 0·39 | 4·10 | 2·06 | 1·86 | 0·44 | 1979 | 6520 | 3·11 | 21·82 | 26·93 | Enr |
| 6K-458-1 | Cpx3 | Ints | 0·790 | 3·28 | 3·01 | 1·46 | 0·48 | 3·09 | 1·58 | 1·53 | 0·57 | 2274 | 8182 | 3·08 | 27·37 | 21·43 | Enr |
| 6K-458-3 | Cpx2 | Ints | 0·332 | 0·69 | 1·41 | 1·25 | 0·46 | 2·82 | 1·43 | 1·26 | 0·40 | 1908 | 5112 | 1·84 | 19·67 | 3·90 | Trans |
| 6K-458-3 | Cpx3 | Core | 0·088 | 0·22 | 1·66 | 1·72 | 0·55 | 3·89 | 1·35 | 1·88 | 0·39 | 2514 | 6894 | 3·81 | 21·41 | 4·96 | Dep |
| 6K-458-3 | Cpx3 | Rim | 0·053 | 0·25 | 1·83 | 1·25 | 0·45 | 3·72 | 1·56 | 1·77 | 0·37 | 2316 | 5660 | 4·76 | 23·93 | 5·28 | Dep |
| 6K-458-3 | Cpx4 | Core | 0·033 | 0·15 | 0·71 | 0·78 | 0·31 | 1·82 | 1·06 | 0·96 | 0·44 | 1374 | 6040 | 3·66 | 13·97 | 1·83 | Dep |
| 6K-458-3 | Cpx4 | Rim | 0·105 | 0·28 | 1·05 | 0·61 | 0·33 | 2·04 | 1·47 | 1·16 | 0·49 | 1541 | 5624 | 2·75 | 15·64 | 3·11 | Dep |
| 6K-458-3 | Cpx5 | Ints | 0·058 | 0·10 | 0·78 | 0·63 | 0·27 | 1·93 | 1·62 | 1·09 | 0·45 | 1934 | 5006 | 4·10 | 16·11 | 3·98 | Dep |
| 6K-458-3 | Cpx6 | Ints | 0·428 | 1·60 | 1·51 | 1·01 | 0·35 | 3·18 | 2·03 | 1·88 | | | | | | | Trans |
| 6K-465-2 | Cpx1 | Core1 | 0·015 | 0·04 | 0·47 | 0·70 | 0·33 | 2·60 | 1·53 | 1·60 | 0·33 | 1312 | 5485 | 3·90 | 15·78 | 1·83 | Dep |
| 6K-465-2 | Cpx1 | Core2 | 0·038 | 0·18 | 0·67 | 0·85 | 0·36 | 2·68 | 1·83 | 1·59 | | | | | | | Dep |
| 6K-465-2 | Cpx1 | Rim1 | 0·008 | 0·05 | 0·71 | 0·90 | 0·30 | 3·31 | 1·82 | 1·72 | 0·31 | 1858 | 5802 | 2·81 | 20·02 | 2·69 | Dep |
| 6K-465-2 | Cpx1 | Rim2 | 0·029 | 0·04 | 0·53 | 0·73 | 0·21 | 1·82 | 1·23 | 0·89 | | | | | | | Dep |
| 6K-465-2 | Cpx2 | Core1 | 0·005 | 0·03 | 0·37 | 0·47 | 0·20 | 1·64 | 1·13 | 1·10 | 0·22 | 1003 | 4291 | 1·16 | 6·63 | 0·80 | Dep |
| 6K-465-2 | Cpx2 | Core2 | 0·002 | 0·03 | 0·31 | 0·44 | 0·20 | 1·29 | 0·84 | 0·90 | 0·28 | 1169 | | 1·59 | 12·22 | 1·66 | Dep |
| 6K-465-2 | Cpx2 | Core3 | 0·005 | 0·05 | 0·40 | 0·44 | 0·22 | 1·44 | 0·71 | 0·77 | 0·27 | 1183 | | 1·08 | 11·40 | 1·30 | Dep |
| 6K-465-2 | Cpx2 | Core4 | 0·004 | 0·03 | 0·32 | 0·57 | 0·22 | 1·51 | 0·83 | 1·00 | | | | | | | Dep |
| 6K-465-2 | Cpx2 | Core5 | 0·011 | 0·02 | 0·30 | 0·49 | 0·27 | 1·77 | 1·09 | 1·07 | | | | | | | Dep |
| 6K-465-2 | Cpx2 | Rim | 0·004 | 0·04 | 0·47 | 0·65 | 0·17 | 2·16 | 1·17 | 1·26 | 0·26 | 1584 | | 6·17 | 16·97 | 2·19 | Dep |
| 6K-465-2 | Cpx3 | Core | 0·017 | 0·04 | 0·41 | 0·48 | 0·24 | 1·97 | 1·01 | 1·19 | 0·22 | 1073 | 4669 | 1·32 | 10·13 | 1·33 | Dep |
| 6K-465-2 | Cpx3 | Rim | 0·016 | 0·04 | 0·50 | 0·75 | 0·26 | 2·64 | 1·60 | 1·57 | 0·24 | 1774 | 4506 | 1·33 | 14·95 | 1·61 | Dep |
| 6K-465-2 | Cpx4 | Core | 0·007 | 0·03 | 0·40 | 0·56 | 0·29 | 2·54 | 1·63 | 1·73 | 0·29 | 1681 | 6007 | 1·47 | 23·18 | 2·93 | Dep |
| 6K-465-2 | Cpx4 | Rim | 0·012 | 0·05 | 0·45 | 0·41 | 0·16 | 1·68 | 0·98 | 1·11 | 0·30 | 1825 | 6264 | 3·42 | 21·05 | 2·88 | Dep |
| 6K-465-2 | Cpx5 | Core1 | 0·863 | 3·77 | 2·48 | 1·10 | 0·38 | 2·69 | 1·92 | 1·98 | 0·52 | 1437 | 5768 | 2·27 | 27·20 | 7·13 | Enr |
| 6K-465-2 | Cpx5 | Core2 | 0·971 | 4·29 | 2·86 | 1·41 | 0·53 | 3·59 | 2·78 | 2·87 | 0·36 | 1283 | | 1·27 | 22·06 | 2·92 | Enr |
| 6K-465-2 | Cpx5 | Rim | 0·470 | 2·09 | 1·82 | 1·27 | 0·38 | 3·17 | 2·65 | 2·42 | 0·17 | 1877 | | 1·17 | 38·52 | 11·86 | Enr |
| 6K-465-2 | Cpx6 | Core1 | 0·120 | 0·32 | 0·47 | 0·50 | 0·22 | 1·63 | 1·08 | 0·97 | 0·29 | 1069 | | 1·02 | 13·14 | 1·19 | Trans |
| 6K-465-2 | Cpx6 | Mdpt2 | 0·048 | 0·14 | 0·45 | 0·52 | 0·26 | 1·69 | 1·02 | 1·09 | 0·37 | 1143 | | 1·28 | 13·21 | 1·21 | Trans |
| 6K-465-2 | Cpx6 | Mdpt3 | 0·159 | 0·62 | 0·73 | 0·69 | 0·26 | 2·34 | 1·53 | 1·83 | 0·37 | 1442 | 5376 | 3·21 | 22·45 | 3·49 | Trans |
| 6K-465-2 | Cpx6 | Mdpt4 | 0·064 | 0·11 | 0·35 | 0·56 | 0·26 | 1·64 | 1·02 | 0·86 | 0·30 | 1001 | | 0·98 | 11·30 | 1·12 | Trans |
| 6K-465-2 | Cpx6 | Mdpt5 | 0·099 | 0·23 | 0·47 | 0·52 | 0·28 | 1·54 | 1·09 | 0·91 | 0·30 | 1053 | | 1·01 | 13·07 | 1·27 | Trans |
| 6K-465-2 | Cpx6 | Mdpt6 | 0·182 | 0·71 | 0·67 | 0·64 | 0·25 | 1·83 | 1·34 | 1·42 | 0·29 | 1108 | | 1·13 | 14·55 | 1·45 | Trans |
| 6K-465-2 | Cpx6 | Mdpt7 | 0·383 | 1·34 | 1·14 | 0·72 | 0·25 | 2·39 | 1·63 | 2·24 | 0·41 | 1426 | 5305 | 1·72 | 26·16 | 3·58 | Trans |
| 6K-465-2 | Cpx6 | Rim8 | 0·377 | 1·73 | 2·17 | 1·10 | 0·32 | 2·71 | 1·77 | 1·97 | 0·27 | 1233 | | 0·93 | 21·25 | 4·69 | Trans |
| 6K-465-2 | Cpx6 | Rim9 | 0·412 | 2·05 | 1·77 | 0·99 | 0·30 | 3·12 | 2·21 | 2·78 | 0·48 | 1774 | 6731 | 3·06 | 30·18 | 7·65 | Trans |
| 6K-465-2 | Cpx7 | Core | 0·169 | 0·60 | 0·81 | 0·73 | 0·35 | 2·40 | 1·93 | 1·70 | | | | | | | Enr |
| 6K-465-2 | Cpx7 | Rim | 0·164 | 0·65 | 0·77 | 0·48 | 0·29 | 2·06 | 1·55 | 1·40 | | | | | | | Enr |
| 6K-465-2 | Cpx8 | Core1 | 0·021 | 0·08 | 0·50 | 0·69 | 0·33 | 2·05 | 1·28 | 1·19 | 0·43 | 1222 | | 0·92 | 14·25 | 1·24 | Dep |
| 6K-465-2 | Cpx8 | Core2 | 0·021 | 0·06 | 0·48 | 0·52 | 0·18 | 1·30 | 0·92 | 0·64 | 0·42 | 1186 | | 1·26 | 13·19 | 1·37 | Dep |
| 6K-465-2 | Cpx8 | Core3 | 0·021 | 0·06 | 0·39 | 0·49 | 0·26 | 1·48 | 1·02 | 0·92 | | | | | | | Dep |
| 6K-465-2 | Cpx8 | Rim1 | 0·071 | 0·22 | 0·44 | 0·45 | 0·20 | 1·50 | 1·10 | 0·87 | | | | | | | Dep |

(continued)

*Table 8: Continued*

| Sample | Grain | Type[a] | La | Ce | Nd | Sm | Eu | Dy | Er | Yb | Na$_2$O | Ti | Cr | Sr | Y | Zr | Notes[†] |
|---|---|---|---|---|---|---|---|---|---|---|---|---|---|---|---|---|---|
| 6K-465-2 | Cpx8 | Rim2 | 0·068 | 0·33 | 0·75 | 0·58 | 0·28 | 2·23 | 1·70 | 1·29 | 0·38 | 1528 | | 0·83 | 18·63 | 1·76 | Dep |
| 6K-465-2 | Cpx8 | Rim3 | 0·089 | 0·34 | 0·76 | 0·72 | 0·30 | 2·41 | 1·71 | 1·67 | 0·40 | 1597 | | 0·80 | 18·87 | 1·75 | Dep |
| 6K-465-2 | Cpx9 | Rim1 | 0·601 | 2·98 | 2·72 | 1·24 | 0·28 | 3·15 | 2·11 | 1·95 | 0·40 | 1396 | 5186 | 2·69 | 28·75 | 10·15 | Enr |
| 6K-465-2 | Cpx9 | Rim2 | 0·941 | 5·33 | 4·84 | 2·23 | 0·51 | 5·31 | 4·17 | 3·76 | 0·33 | 1398 | | 1·03 | 31·12 | 9·39 | Enr |
| 6K-465-2 | Cpx9 | Rim3 | 1·344 | 7·99 | 7·57 | 3·83 | 0·79 | 7·78 | 5·58 | 5·46 | 0·37 | 2075 | | 1·41 | 42·81 | 16·63 | Enr |
| 6K-465-2 | Cpx10 | Ints | 0·009 | 0·04 | 0·49 | 0·78 | 0·24 | 3·08 | 1·82 | 1·50 | 0·34 | 1705 | 4662 | 3·45 | 9·89 | 1·32 | Dep |
| 6K-465-2 | Cpx11 | Core1 | 0·007 | 0·06 | 0·54 | 0·81 | 0·29 | 2·05 | 1·31 | 1·35 | | | | | | | Dep |
| 6K-465-2 | Cpx11 | Core2 | 0·007 | 0·05 | 0·50 | 0·66 | 0·23 | 2·21 | 1·31 | 1·24 | | | | | | | Dep |
| 6K-465-2 | Cpx11 | Rim | 0·005 | 0·05 | 0·44 | 0·57 | 0·19 | 1·95 | 1·16 | 1·12 | | | | | | | Dep |
| 6K-465-2 | Cpx12 | Ints | 0·010 | 0·04 | 0·42 | 0·52 | 0·23 | 1·94 | 1·24 | 1·29 | | | | | | | Dep |
| RC27-9-6-5 | Cpx1 | Core1 | 0·861 | 2·77 | 1·54 | 0·64 | 0·36 | 1·77 | 1·17 | 1·23 | 0·29 | 1273 | 5768 | 1·63 | 18·74 | 4·23 | Enr |
| RC27-9-6-5 | Cpx1 | Core2 | 0·858 | 2·29 | 1·45 | 0·66 | 0·36 | 2·04 | 0·98 | 1·36 | 0·48 | 1194 | 6389 | 2·26 | 14·35 | 1·05 | Enr |
| RC27-9-6-5 | Cpx1 | Rim | 1·124 | 6·93 | 9·11 | 4·01 | 0·98 | 5·65 | 2·75 | 2·00 | 0·24 | 3659 | 4979 | 3·15 | 42·21 | 82·90 | Enr |
| RC27-9-6-5 | Cpx2 | Core1 | 0·021 | 0·05 | 0·25 | 0·30 | 0·16 | 1·12 | 0·64 | 0·73 | 0·36 | 1007 | 5579 | 0·83 | 11·61 | 1·08 | Trans |
| RC27-9-6-5 | Cpx2 | Mdpt2 | | | | | | | | | 0·30 | 1070 | 6809 | 1·73 | 13·86 | 1·14 | Trans |
| RC27-9-6-5 | Cpx2 | Mdpt3 | 0·060 | 0·13 | 0·20 | 0·36 | 0·17 | 1·43 | 0·84 | 0·76 | 0·39 | 1121 | 5698 | 1·28 | 13·07 | 1·17 | Trans |
| RC27-9-6-5 | Cpx2 | Mdpt4 | 0·194 | 0·37 | 0·42 | 0·38 | 0·18 | 1·66 | 0·88 | 0·90 | 0·36 | 1270 | 7237 | 1·91 | 16·11 | 1·30 | Trans |
| RC27-9-6-5 | Cpx2 | Mdpt5 | 0·879 | 3·74 | 2·35 | 1·27 | 0·45 | 2·59 | 1·67 | 1·63 | 0·39 | 1544 | 6811 | 2·40 | 26·81 | 13·06 | Trans |
| RC27-9-6-5 | Cpx2 | Mdpt6 | 0·999 | 4·40 | 3·51 | 1·35 | 0·48 | 3·06 | 1·76 | 1·66 | 0·41 | 1873 | 6857 | 2·16 | 29·80 | 18·35 | Trans |
| RC27-9-6-5 | Cpx2 | Rim7 | 1·001 | 5·21 | 5·37 | 2·20 | 0·62 | 4·57 | 2·32 | 1·98 | 0·31 | 2792 | 4956 | 1·92 | 31·24 | 45·18 | Trans |
| RC27-9-6-5 | Cpx3 | Ints | 1·004 | 7·00 | 9·36 | 4·96 | 0·99 | 6·44 | 2·78 | 2·43 | 1·19 | 7912 | 6282 | 9·01 | 58·17 | 150·43 | Enr |
| RC27-9-6-5 | Cpx4 | Core | 1·311 | 6·33 | 4·68 | 1·74 | 0·62 | 3·24 | 1·56 | 1·51 | 0·55 | 1471 | 5683 | 2·26 | 23·67 | 16·90 | Enr |
| RC27-9-6-5 | Cpx4 | Rim | 1·001 | 4·58 | 5·23 | 1·97 | 0·61 | 3·69 | 1·83 | 1·53 | 0·35 | 2646 | 5562 | 2·97 | 30·66 | 51·25 | Enr |
| RC27-9-6-5 | Cpx5 | Core | 1·446 | 6·11 | 3·30 | 0·96 | 0·51 | 2·35 | 1·41 | 1·49 | 0·77 | 1632 | 6555 | 3·24 | 25·19 | 21·34 | Enr |
| RC27-9-6-5 | Cpx5 | Rim | 1·141 | 5·69 | 5·93 | 2·65 | 0·65 | 4·16 | 2·32 | 2·12 | 0·50 | 2776 | 8399 | 2·38 | 37·76 | 53·11 | Enr |

[*]Ints refers to interstitial grain, <1 mm diameter. Numbered analyses and Mdpt (midpoint between core and rim) refer to multiple analyses of grains in cryptically metasomatized samples.
[†]Dep, Trans and Enr are depleted, transitional and enriched zones in cryptically metasomatized samples; blank indicates residual peridotite.
[‡]Cpx from Kilbourne Hole (Irving & Frey, 1984), used as a standard for REE.
[§]Kilauea tholeiitic basalt glass (Jochum *et al.*, 2000), used as a standard for the other trace elements.
[¶]Per cent error based on average counting error among Cpx analyses, including unpublished analyses.
[**]Per cent error based on average difference among duplicate Cpx analyses, including unpublished duplicate pairs.

*Table 9: Ion probe trace element concentrations (in ppm) for residual peridotite Cpx*

| Sample | Grain[*] | Type[†] | La | Ce | Nd | Sm | Eu | Dy | Er | Yb | Na$_2$O | Ti | Cr | Sr | Y | Zr |
|---|---|---|---|---|---|---|---|---|---|---|---|---|---|---|---|---|
| 6K-466-1 | Cpx1 | Core | 0·011 | 0·06 | 0·41 | 0·49 | 0·20 | 1·57 | 0·70 | 0·91 | 0·46 | 1294 | 9529 | 1·22 | 10·77 | 2·31 |
| 6K-466-1 | Cpx1 | Rim | 0·005 | 0·05 | 0·52 | 0·39 | 0·17 | 1·75 | 0·89 | 0·75 | 0·41 | 1400 | 8847 | 1·61 | 12·37 | 2·53 |
| 6K-466-1 | Cpx3 | Ints | 0·064 | 0·07 | 0·47 | 0·38 | 0·20 | 1·50 | 0·85 | 0·79 | 0·40 | 1480 | 8195 | 1·77 | 11·77 | 2·89 |
| 6K-466-1 | Cpx3D | Ints | | | | | | | | | 0·39 | 1628 | 8259 | 2·38 | 12·75 | 3·59 |
| 6K-643-1 | Cpx1 | Ints | 0·024 | 0·04 | 0·23 | 0·29 | 0·15 | 1·74 | 0·93 | 1·30 | 0·20 | 913 | 6261 | 1·15 | 9·90 | 0·94 |
| 6K-643-1 | Cpx1D | Ints | 0·016 | 0·02 | 0·25 | 0·32 | 0·26 | 2·36 | 1·26 | 1·60 | 0·18 | 1032 | 6518 | 1·41 | 10·39 | 0·90 |
| 6K-643-1 | Cpx2 | Core | 0·018 | 0·04 | 0·26 | 0·25 | 0·18 | 1·37 | 0·94 | 0·85 | 0·21 | 579 | 5425 | 1·27 | 5·30 | 0·66 |
| 6K-643-1 | Cpx2 | Rim | 0·023 | 0·04 | 0·20 | 0·25 | 0·12 | 0·83 | 0·61 | 0·54 | 0·34 | 918 | 5538 | 1·39 | 8·98 | 1·00 |

(continued)

*Table 9: Continued*

| Sample | Grain* | Type† | La | Ce | Nd | Sm | Eu | Dy | Er | Yb | Na$_2$O | Ti | Cr | Sr | Y | Zr |
|---|---|---|---|---|---|---|---|---|---|---|---|---|---|---|---|---|
| 6K-643-1 | Cpx4 | Core | 0·025 | 0·04 | 0·25 | 0·33 | 0·15 | 0·92 | 0·65 | 0·65 | 0·42 | 809 | 5284 | 1·33 | 9·26 | 1·87 |
| 6K-643-1 | Cpx4 | Rim | 0·023 | 0·04 | 0·39 | 0·39 | 0·19 | 1·35 | 0·95 | 0·81 | 0·35 | 714 | 4664 | 1·63 | 7·01 | 1·31 |
| 6K-643-1 | Cpx8 | Symp | 0·019 | 0·06 | 0·31 | 0·45 | 0·16 | 1·34 | 0·71 | 0·80 | 0·29 | 905 | 5245 | 1·41 | 8·71 | 1·71 |
| 6K-643-1 | Cpx8D | Symp | 0·017 | 0·06 | 0·28 | 0·54 | 0·17 | 1·49 | 0·83 | 0·92 | 0·31 | 1261 | 4916 | 1·78 | 12·00 | 1·12 |
| 6K-643-6 | Cpx5 | Ints | 0·027 | 0·05 | 0·20 | 0·25 | 0·13 | 0·86 | 0·54 | 0·51 | 0·44 | 1233 | 9453 | 2·39 | 8·26 | 1·69 |
| 6K-643-6 | Cpx6 | Ints | 0·020 | 0·05 | 0·15 | 0·32 | 0·12 | 0·92 | 0·58 | 0·55 | 0·48 | 1223 | 10072 | 1·81 | 8·37 | 6·04 |
| 6K-643-13 | Cpx1 | Ints | 0·007 | 0·01 | 0·10 | 0·30 | 0·10 | 0·97 | 0·71 | 0·63 | 0·30 | 961 | 5195 | 1·90 | 9·95 | 0·73 |
| 6K-643-13 | Cpx2 | Core | 0·021 | 0·02 | 0·17 | 0·31 | 0·23 | 1·42 | 0·82 | 0·88 | 0·13 | 602 | 5945 | 1·25 | 5·23 | 0·66 |
| 6K-643-13 | Cpx2 | Rim | 0·02 | 0·09 | 0·28 | 0·09 | 1·33 | 0·89 | 0·75 | 0·24 | 877 | 6416 | 1·60 | 9·60 | 0·73 | |
| 6K-643-13 | Cpx3 | Ints | 0·004 | 0·03 | 0·11 | 0·15 | 0·08 | 0·87 | 0·63 | 0·46 | 0·28 | 1047 | 3633 | 1·68 | 8·53 | 0·76 |
| 6K-649-5 | Cpx1 | Core | 0·005 | 0·00 | 0·22 | 0·26 | 0·13 | 1·13 | 0·85 | 0·96 | 0·26 | 683 | 6554 | 2·20 | 9·12 | 0·65 |
| 6K-649-5 | Cpx1 | Rim | 0·032 | 0·02 | 0·25 | 0·27 | 0·17 | 1·33 | 0·92 | 0·91 | 0·27 | 802 | 5774 | 1·60 | 9·62 | 0·95 |
| 6K-649-5 | Cpx2 | Ints | 0·025 | 0·04 | 0·15 | 0·23 | 0·13 | 1·42 | 0·66 | 0·96 | 0·17 | 947 | 11618 | 1·26 | 13·05 | 1·17 |
| 6K-649-5 | Cpx4 | Ints | 0·020 | 0·03 | 0·23 | 0·25 | 0·12 | 1·28 | 0·85 | 1·04 | | | | | | |
| 6K-649-5 | Cpx5 | Core | 0·016 | 0·02 | 0·10 | 0·15 | 0·09 | 1·17 | 0·67 | 0·95 | | | | | | |
| 6K-649-5 | Cpx5 | Rim | 0·016 | 0·02 | 0·22 | 0·17 | 0·13 | 1·40 | 0·77 | 1·06 | | | | | | |
| 6K-649-5 | Cpx6 | Ints | 0·012 | 0·02 | 0·16 | 0·12 | 0·07 | 0·94 | 0·53 | 1·04 | 0·30 | 756 | 4771 | 1·28 | 8·10 | 1·17 |
| 6K-649-5 | Cpx7 | Ints | 0·015 | 0·01 | 0·11 | 0·08 | 0·06 | 0·87 | 0·49 | 0·76 | | | | | | |
| 6K-649-5 | Cpx8 | Ints | 0·007 | 0·02 | 0·18 | 0·24 | 0·08 | 1·32 | 0·84 | 1·01 | | | | | | |
| 6K-649-5 | Cpx9 | Ints | 0·021 | 0·02 | 0·17 | 0·15 | 0·11 | 1·35 | 0·71 | 1·01 | 0·33 | 748 | 4813 | 3·71 | 8·20 | 2·24 |
| JR31-52-3 | Cpx4 | Core | 0·007 | 0·03 | 0·27 | 0·38 | 0·19 | 1·36 | 0·77 | 0·78 | 0·53 | 912 | 10956 | 0·96 | 11·03 | 0·87 |
| JR31-52-3 | Cpx4 | Rim | 0·009 | 0·06 | 0·26 | 0·43 | 0·17 | 1·61 | 0·77 | 0·79 | 0·51 | 941 | 10004 | 0·86 | 11·15 | 0·91 |
| JR31-52-3 | Cpx5 | Core | 0·012 | 0·03 | 0·22 | 0·34 | 0·13 | 1·09 | 0·62 | 0·63 | | | | | | |
| JR31-52-3 | Cpx5 | Rim | 0·015 | 0·03 | 0·26 | 0·31 | 0·18 | 1·01 | 0·63 | 0·62 | | | | | | |
| JR31-52-3 | Cpx5D | Rim | 0·011 | 0·05 | 0·29 | 0·39 | 0·17 | 1·18 | 0·65 | 0·63 | | | | | | |
| JR31-52-3 | Cpx6 | Ints | 0·008 | 0·05 | 0·30 | 0·31 | 0·17 | 1·15 | 0·64 | 0·61 | | | | | | |
| JR31-52-3 | Cpx7 | Core | 0·005 | 0·03 | 0·35 | 0·47 | 0·16 | 1·19 | 0·74 | 0·71 | 0·50 | 904 | 10097 | 0·93 | 10·13 | 0·90 |
| JR31-52-3 | Cpx7 | Rim | 0·030 | 0·04 | 0·34 | 0·36 | 0·20 | 1·41 | 0·83 | 0·84 | 0·49 | 1071 | 8866 | 1·15 | 10·40 | 0·96 |
| JR31-52-3 | Cpx9 | Ints | 0·001 | 0·03 | 0·26 | 0·30 | 0·19 | 1·43 | 0·80 | 0·81 | 0·48 | 1018 | 8834 | 1·35 | 10·20 | 0·82 |
| JR31-52-4 | Cpx3 | Core | 0·001 | 0·01 | 0·16 | 0·21 | 0·06 | 0·65 | 0·38 | 0·32 | | | | | | |
| JR31-52-4 | Cpx3 | Rim | 0·002 | 0·03 | 0·31 | 0·23 | 0·10 | 0·72 | 0·55 | 0·52 | | | | | | |
| JR31-52-4 | Cpx4 | Core | 0·005 | 0·03 | 0·33 | 0·40 | 0·15 | 1·34 | 0·86 | 0·71 | 0·39 | 1052 | 10374 | 0·89 | 12·14 | 0·81 |
| JR31-52-4 | Cpx4 | Rim | 0·005 | 0·03 | 0·34 | 0·40 | 0·15 | 1·38 | 0·84 | 0·70 | 0·30 | 1426 | 13683 | 1·12 | 16·93 | 1·26 |
| JR31-52-5 | Cpx1 | Core | 0·005 | 0·02 | 0·30 | 0·49 | 0·20 | 1·43 | 0·77 | 0·76 | 0·43 | 920 | 10969 | 0·59 | 12·06 | 1·04 |
| JR31-52-5 | Cpx1 | Rim | 0·008 | 0·01 | 0·26 | 0·34 | 0·22 | 1·39 | 0·77 | 0·82 | 0·29 | 1126 | 7950 | 0·64 | 12·58 | 1·36 |
| JR31-52-5 | Cpx3 | Core | 0·011 | 0·02 | 0·28 | 0·42 | 0·21 | 1·52 | 0·89 | 0·88 | 0·35 | 1126 | 10428 | 1·23 | 14·01 | 0·88 |
| JR31-52-5 | Cpx5 | Ints | 0·009 | 0·02 | 0·21 | 0·33 | 0·12 | 1·00 | 0·69 | 0·61 | 0·39 | 1002 | 8800 | 0·91 | 11·27 | 0·85 |
| JR31-52-8 | Cpx1 | Core | 0·008 | 0·02 | 0·25 | 0·27 | 0·16 | 1·12 | 0·64 | 0·71 | 0·37 | 730 | 10371 | 0·52 | 7·62 | 0·61 |
| JR31-52-8 | Cpx1 | Rim | 0·009 | 0·04 | 0·31 | 0·32 | 0·18 | 1·29 | 0·86 | 0·70 | 0·47 | 1097 | 9310 | 0·87 | 10·98 | 0·75 |
| JR31-52-8 | Cpx1D | Rim | 0·006 | 0·04 | 0·34 | 0·41 | 0·21 | 1·48 | 0·77 | 0·82 | | | | | | |
| JR31-52-8 | Cpx3 | Ints | 0·013 | 0·04 | 0·41 | 0·44 | 0·17 | 1·39 | 0·79 | 0·72 | 0·50 | 1213 | 11035 | 0·99 | 12·42 | 0·99 |
| JR31-52-8 | Cpx4 | Rim | 0·006 | 0·04 | 0·30 | 0·40 | 0·16 | 1·36 | 0·83 | 0·92 | 0·42 | 959 | 5842 | 2·02 | 8·68 | 0·78 |
| JR31-52-8 | Cpx5 | Ints | 0·029 | 0·07 | 0·46 | 0·49 | 0·23 | 1·52 | 0·92 | 0·85 | 0·48 | 1086 | 10099 | 0·91 | 10·48 | 0·83 |
| RC27-9-6-7 | Cpx1 | Core | 0·011 | 0·05 | 0·21 | 0·49 | 0·20 | 1·04 | 0·52 | 0·48 | 0·12 | 387 | 4695 | 1·31 | 3·37 | 0·72 |
| RC27-9-6-7 | Cpx1 | Rim | 0·003 | 0·05 | 0·52 | 0·72 | 0·24 | 1·59 | 0·96 | 0·72 | 0·31 | 1235 | 4952 | 1·82 | 12·74 | 1·52 |
| RC27-9-6-7 | Cpx3 | Ints | 0·008 | 0·04 | 0·22 | 0·52 | 0·22 | 1·65 | 0·73 | 0·83 | 0·29 | 1196 | 4220 | 1·39 | 11·13 | 1·26 |
| RC27-9-6-7 | Cpx5 | Ints | 0·014 | 0·04 | 0·44 | 0·73 | 0·32 | 2·18 | 1·06 | 0·87 | 0·43 | 1515 | 4490 | 1·63 | 12·59 | 1·70 |

*D following a grain number indicates duplicate analysis.
†Ints refers to interstitial grain, <1 mm diameter; Symp refers to symplectite.

*Table 10: Ion probe trace element concentrations (in ppm) for cryptically metasomatized peridotite Plag*

| | Grain* | La | Ce | Nd | Sm | Eu | Dy | Er | Yb | Na$_2$O | Ti | Cr | Sr | Y | Zr |
|---|---|---|---|---|---|---|---|---|---|---|---|---|---|---|---|
| Count error (%):† | Plag | 8 | 5 | 10 | 23 | 7 | 28 | 22 | 31 | 0 | 3 | 12 | 3 | 14 | 21 |
| *Sample* | | | | | | | | | | | | | | | |
| 6K-465-2 | Plag1 | | | | | | | | | 1·33 | | | 57·8 | 0·95 | |
| 6K-465-2 | Plag2 | | | | | | | | | 0·24 | | | 38·6 | 0·35 | |
| 6K-465-2 | Plag3 | | | | | | | | | 0·94 | 52 | | 2·5 | 0·33 | 0·41 |
| 6K-465-2 | Plag4 | | | | | | | | | 1·02 | 52 | | 1·4 | 0·18 | 0·33 |
| 6K-465-2 | Plag5 | | | | | | | | | 1·02 | 60 | | 31·8 | 0·29 | 0·37 |
| 6K-465-2 | Plag6 | | | | | | | | | 0·96 | 52 | | 1·3 | 0·34 | 0·46 |
| RC27-9-6-5 | Plag1 | 1·23 | 1·73 | 0·27 | 0·02 | 0·23 | 0·01 | 0·08 | 0·02 | 1·59 | 36 | 2·58 | 6·5 | 0·06 | 0·12 |

*All grains are interstitial and from the depleted zones of cryptically metasomatized peridotites.
†Per cent error based on average counting error among plagioclase analyses, including unpublished analyses.
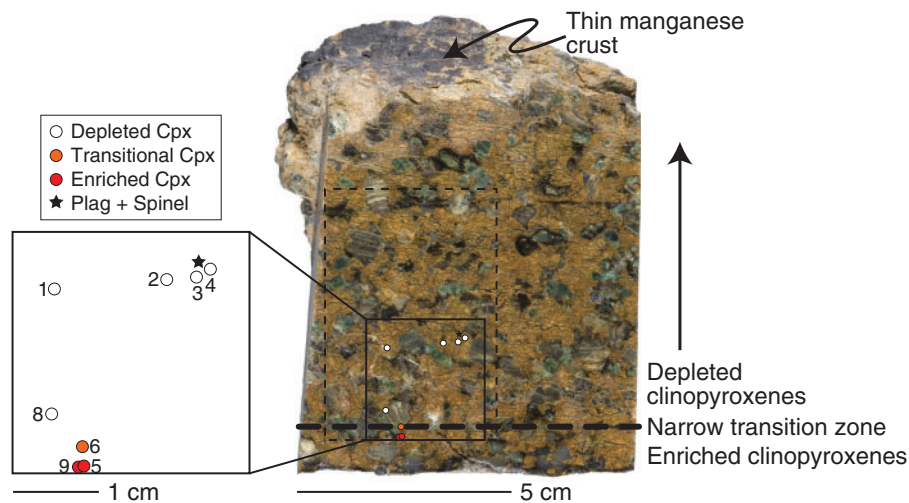


**Fig. 2.** Photograph of cryptically metasomatized peridotite 6K-465-2 from the ridge–transform intersection of the Atlantis II Fracture Zone. The hand specimen looks like a typical residual abyssal peridotite and has no unusual characteristics such as melt veins. However, Cpx LREE concentrations vary across the sample by 2–3 orders of magnitude. The dashed rectangle indicates the area of the rock studied in thin section, with circles to indicate the location of Cpx analyses. As the thin section was cut 2 cm higher than the surface of the slab shown here, Cpx analytical locations do not necessarily correspond to Cpx in the photograph. The box is enlarged to show the location of Cpx grains analyzed for trace elements by ion microprobe. Numbers correspond to Cpx grain numbers in Tables 3 and 8. The star indicates the location of the spinel and plagioclase cluster shown in Fig. 3d. The transition from depleted Cpx (low LREE concentrations) to enriched Cpx (high LREE concentrations) occurs over a distance of <1 cm. Photo courtesy of Tom Kleindinst.

fine-grained shear zone in RC27-9-6-5 does not contain Cpx.

Overall, in none of the four enriched samples in this study is the cryptic metasomatism interpreted as originating from veins or dikelets within the samples. However, as will be discussed below, the metasomatic enrichments must have originated from a nearby vein or network of veins. Among the other samples in the dives and dredge that contain the metasomatized peridotites, there is evidence for the presence of melt. In addition to the two metasomatized peridotites in Dive 458, a further two peridotites and two oxide gabbros were recovered. Dive 465 recovered a mix of peridotite, serpentinite, olivine gabbro and diabase. Of particular note is sample 6K-465-3, a peridotite with at least two generations of gabbro veins of highly evolved compositions that include minerals such as apatite, rutile and ilmenite. In dredge RC27-9-6, only peridotite and dunite were recovered. However, one of the peridotites has a clinopyroxenite vein, discussed by Warren *et al.* (2009), and another sample contains a
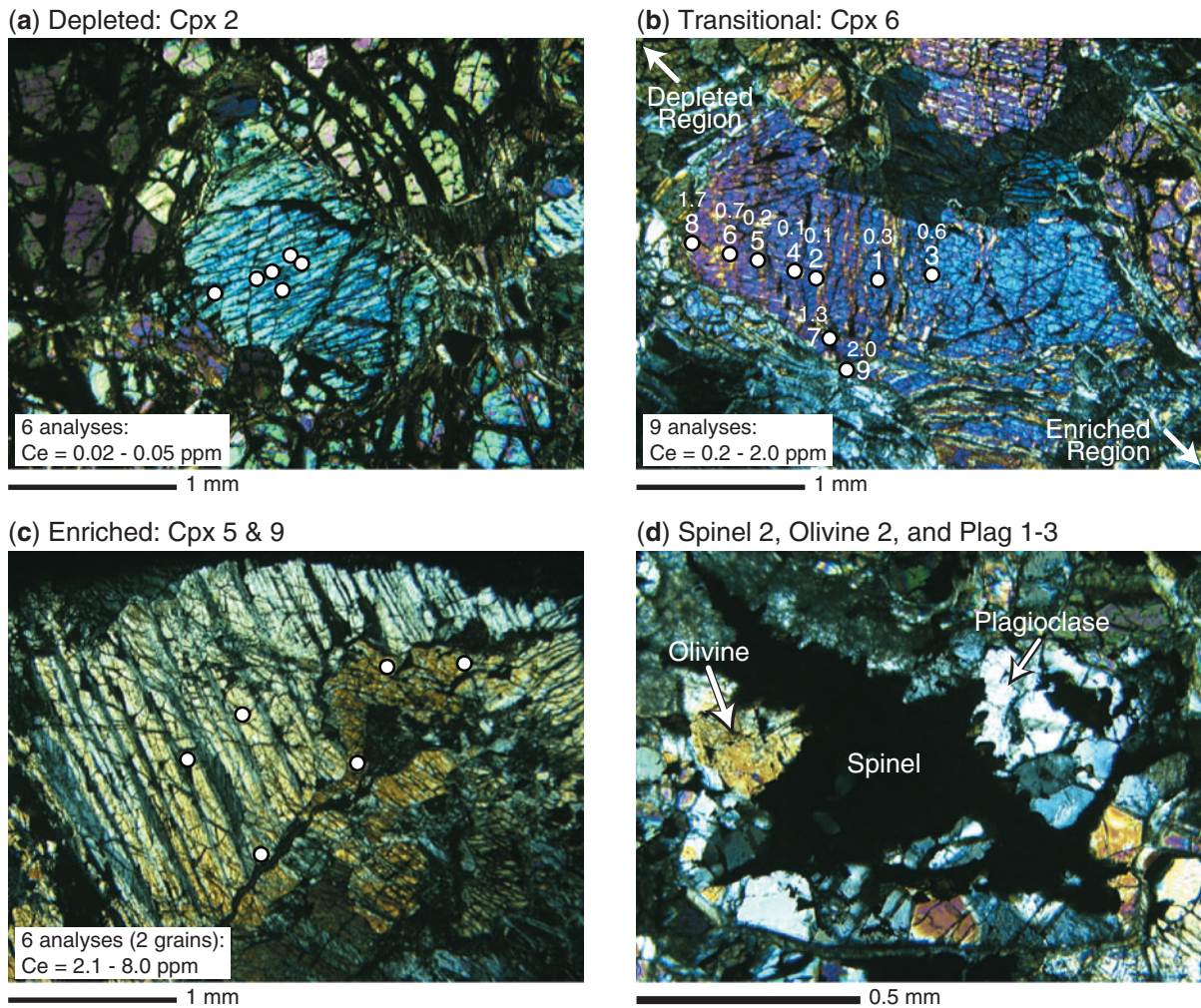
**Fig. 3.** Photomicrographs from cryptically metasomatized peridotite 6K-465-2; white dots indicate trace element analysis locations. (a) Photomicrograph of Cpx 2, a porphyroclast from the depleted portion of the peridotite, surrounded by olivine and serpentine. (b) Photomicrograph of compositionally zoned Cpx 6, located in the transition zone between the depleted and enriched regions of the peridotite. The grain is surrounded by olivine, Cpx and serpentine. Numbering of analytical points corresponds to the numbering in Tables 3 and 8. Smaller numbers are Ce concentrations in ppm. The lowest trace element concentrations are centered around Point 4. Point 3, although appearing to be near the gain center, has higher concentrations, suggesting that in the third dimension it is closer to the grain rim. (c) Photomicrograph of Cpx 5 (large porphyroclast) and Cpx 9 (smaller, darker grain), from the enriched portion of the peridotite. Grains are adjacent to olivine, Cpx and serpentine. (d) Photomicrograph of a spinel, plagioclase and olivine cluster, located in the depleted portion of the peridotite, as shown in Fig. 2.

gabbro vein. Both the dives and the dredge sampled ~1 km of seafloor and better spatial constraints for the relationship between samples within dives or dredges cannot be determined. In the dives, precise sample locations are available, but none of the samples were attached to outcrops and thus they originated at an unknown distance upslope of the sample location.

## Trace elements

Chondrite-normalized REE patterns in Cpx for each of the 10 residual abyssal peridotites are shown in Fig. 5. Cpx REE compositions are compared with the range of other Atlantis II Fracture Zone peridotite Cpx from Johnson &

Dick (1992). In addition, Cpx is compared with the predicted composition of Cpx in the depleted MORB (mid-ocean ridge basalt) mantle (DMM, Workman & Hart, 2005). DMM is a hypothetical composition for the depleted upper mantle, derived from the average isotopic composition of MORB. All 10 peridotites have depleted REE patterns that are within the range of other Atlantis II Fracture Zone peridotite Cpx (Johnson & Dick, 1992).

The REE patterns for the four cryptically metasomatized peridotites are shown in Fig. 6. In three of the samples, trace elements vary spatially from depleted to enriched compositions, as indicated in Fig. 2. Grains located in the transition zone between the enriched and
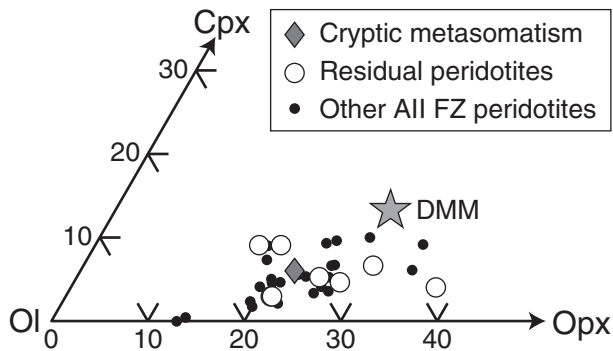
**Fig. 4.** Modal composition of abyssal peridotites in this study compared with other Atlantis II Fracture Zone peridotites. Data for other peridotites are from Johnson & Dick (1992), Kumagai *et al.* (2003) and Morishita *et al.* (2007). The modal composition of DMM is from Workman & Hart (2005). The cryptically metasomatized peridotite has a modal composition similar to that of other Atlantis II peridotites.

depleted portions of the peridotites have core to rim variations in concentration, as shown for a Cpx porphyroclast in Fig. 3c and plotted in Fig. 6. It should be noted that the two-dimensional slice of the Cpx grain in Fig. 3c may not represent a true section through the grain core. As this grain is spatially located at the transition between enriched and depleted portions of the peridotite, this would only indicate that the trace element enrichment did not penetrate deep into the grain. In contrast, other porphyroclasts have similar core and rim concentrations (Table 8), with the entire grain being either enriched or depleted. In sample 6K-458-1, all analyzed Cpx are relatively enriched in REE, with concentrations similar to DMM, but with negative Eu anomalies. As this sample was collected near sample 6K-458-3, which contains both depleted and enriched grains, the enriched trace elements in 6K-458-1 may be related, a possibility that is discussed further below.

Texturally, Cpx in the metasomatized peridotites varies from porphyroclasts to recrystallized grains; the latter are found as aggregates or as elongate grains adjacent to Opx. However, Cpx textures do not correlate with trace elements, with porphyroclastic and interstitial grains having the same trace element concentrations; instead trace elements vary spatially across the thin sections. Three Cpx porphyroclasts from 6K-465-2 that encompass the full range of trace element abundances, but are texturally identical, are shown in Fig. 3a–c. These grains are relatively coarse (1–3 mm), with smoothly curved grain boundaries containing some complex cusps and lobes. The absence of a textural correlation with the trace element abundance variations suggests that the trace element enrichment is unrelated to the melting that initially depleted the peridotite.

In two of the four cryptically metasomatized peridotites, the rims of both depleted and enriched Cpx have negative Eu anomalies, but the cores do not (Fig. 6). Trace amounts

of plagioclase were identified in these samples, present as tiny grains adjacent to spinel and in clusters with olivine (Fig. 3d). The observation of Eu anomalies in rims but not cores of depleted and enriched Cpx suggests that plagioclase formation occurred after the melt–rock reaction event. The trace element concentrations in plagioclase around the spinel grain in Fig. 3d are highly variable, with Sr ranging from 1 to 58 ppm (Table 10).

## Major elements

Mineral phases in the cryptically metasomatized peridotites have mantle major element compositions: olivine is $Fo_{90}$, Opx is Mg-number 90 $[= Mg/(Mg + Fe)]$ and Cpx is Mg-number 91. Plots of Cpx Mg-number against Cr-number $[=Cr/(Cr + Al)]$ and $Na_2O$ in Fig. 7 demonstrate that the cryptically metasomatized peridotites have the same range in major element compositions as other Atlantis II residual peridotites. Some Cpx extend to high Cr-number (= 20), but residual Cpx also extend toward high Cr-number.

Spinel compositions are plotted in Fig. 8. The variation of spinel Cr-number and Mg-number follows the general trend for depletion of peridotites during melting, with Cr-number increasing during melting whereas Mg-number decreases over a more limited range (Dick & Bullen, 1984). Spinels from Atlantis II tend to have low Cr-number (typically <30) and high Mg-number (typically >70), suggesting a limited degree of melting. In Fig. 8b, spinel $TiO_2$ is plotted as a function of Cr-number. $TiO_2$ is incompatible in spinel, although its incompatibility may decrease with increasing Cr-number (E. Hellebrand, personal communication). Most spinels that plot off the Cr-number–Mg-number trend also have high $TiO_2$, suggesting that these parameters combined indicate refertilization of the peridotite by differentiated melts.

In the cryptically metasomatized peridotites, spinels are irregularly shaped with deep embayments and generally <1 mm diameter, though some grains reach 5 mm length. Spinel Cr-number varies from 15 to 49 and intra-sample variations in spinel Cr-number are large (Table 6). Grains with high Cr-number tend to have higher $TiO_2$, a further indication that the cryptic metasomatism is the result of melt refertilization. Around some spinels, trace amounts of plagioclase are present as equant intergrowths with olivine around spinel. For example, in sample 6K-465-2, the highest Cr-number spinel is a grain that from textural relationships appears to have reacted with pyroxenes to form the low-pressure assemblage of plagioclase and olivine (Fig. 3).

## DISCUSSION
### Mechanisms of peridotite metasomatism

Mantle melting during adiabatic upwelling beneath mid-ocean ridges is near-fractional, meaning that upward
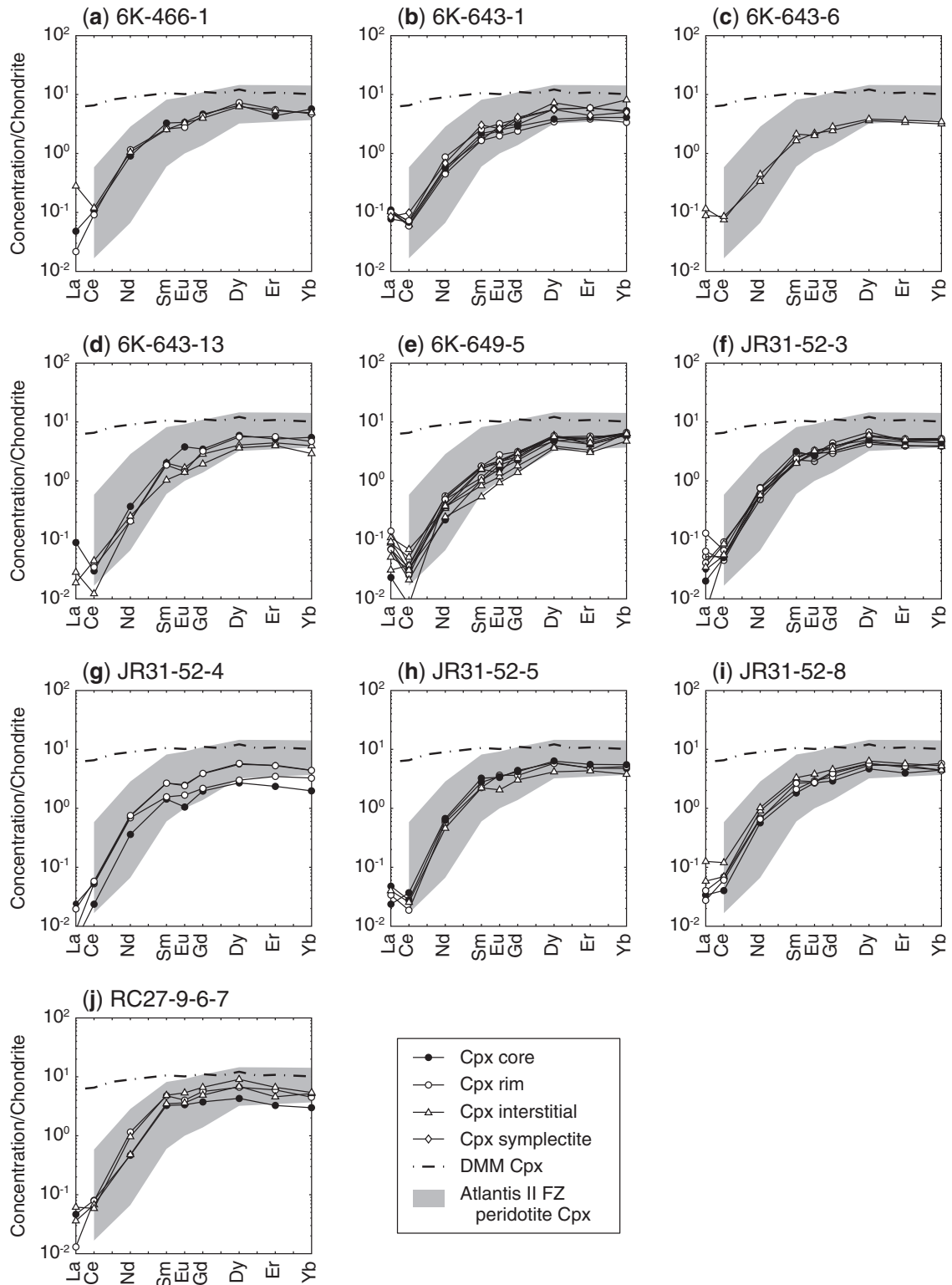
**Fig. 5.** Variation of REE in Cpx from the residual abyssal peridotites in this study. Data are normalized to chondrite (Anders & Grevesse, 1989); the composition of Cpx in DMM is from Workman & Hart (2005); the background dataset is Atlantis II Fracture Zone peridotite Cpx from Johnson & Dick (1992).
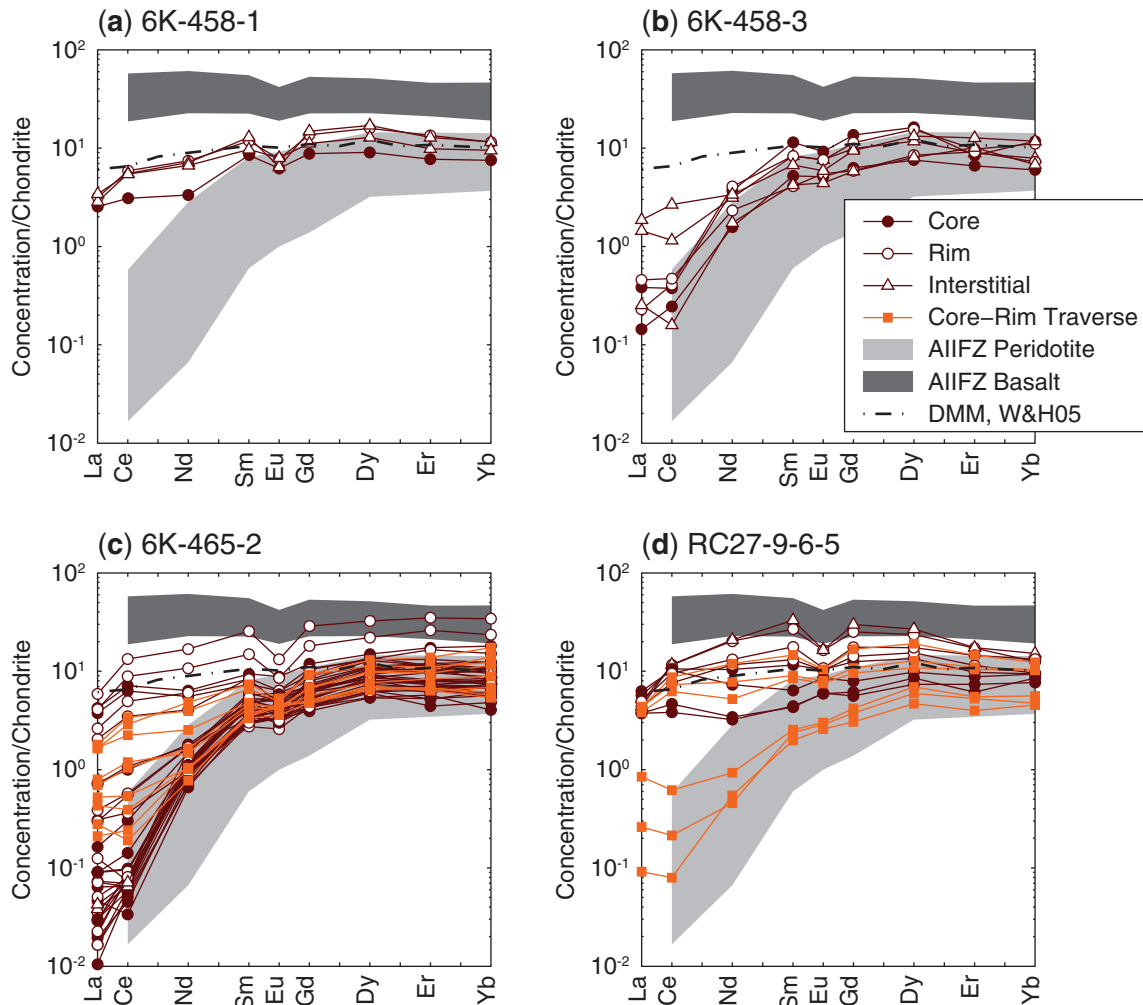
**Fig. 6.** Variation of REE in Cpx from the cryptically metasomatized peridotites. Core to rim traverses of a single Cpx grain in 6K-465-2 and in RC27-9-6-5 are shown in orange. In both grains, the most depleted analyses are in the core and concentrations increase towards the rim. In 6K-465-2, this Cpx is spatially located between depleted and enriched Cpx grains. Analysis locations for this grain are shown in Fig. 3c. Data are normalized to chondrite using Anders & Grevesse (1989), the dashed line is DMM Cpx from Workman and Hart (2005), and the background fields are the Atlantis II Fracture Zone peridotite and basalt datasets from Johnson & Dick (1992).

extraction (migration) of melt from the site of melting should be efficient. As the mantle moves upward, continued melt formation and extraction occurs. Hence, the residual peridotite becomes increasingly more depleted in incompatible elements, as observed in abyssal peridotite Cpx compositions (e.g. Johnson *et al.*, 1990; Hellebrand *et al.*, 2001; Brunelli *et al.*, 2006). At the grain scale, while melt mass is increasing, mantle melting proceeds with continual reaction among peridotite minerals and melt (Liang, 2003).

As melt migration is faster than the upward flow of the residual peridotites, the minerals in the residual peridotites can come into contact with and react with percolating melts under disequilibrium conditions (e.g. Kelemen *et al.*, 1992; Morgan *et al.*, 2008). Reactions between melt and

peridotite can occur regardless of whether melt flow is focused or not, and could take a variety of forms, including dissolution, crystal growth, or chemical exchange between crystals and melt without modal changes, depending on pressure, temperature, melt composition, and melt–rock ratio, among other variables. The observation of pyroxenite and gabbro veins in abyssal peridotites (e.g. Dick, 1989; Dantas *et al.*, 2007; Warren *et al.*, 2009) indicates that melts beneath mid-ocean ridges directly intrude into peridotite, along with forming the melt–rock reaction zones associated with dunites. These veins suggest that the crystallization of melts within the mantle is often an important process at mid-ocean ridges and that melt extraction is not always as efficient as suggested by near-fractional melting models.
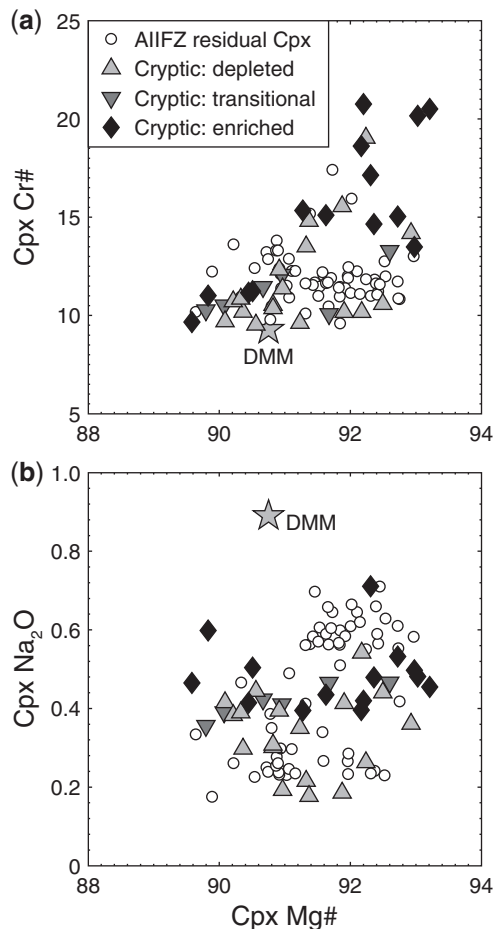
**Fig. 7.** Variation of Mg-number with Cr-number and Na$_2$O in Cpx for residual and cryptically metasomatized peridotites from the Atlantis II Fracture Zone. Additional data from Johnson *et al.* (1990), Johnson & Dick (1992), Coogan *et al.* (2004) and Morishita *et al.* (2007); the composition of DMM Cpx is from Workman & Hart (2005).

The thermal regime of the Atlantis II Fracture Zone is controlled by the low spreading rate (14 mm/year) and the fracture zone, which result in a limited degree of melting because of conductive cooling from above (Bown & White, 1994). Under these conditions, migrating melt is cooled and melt extraction is expected to be incomplete. In abyssal peridotites, evidence for incomplete melt extraction at low and high melt/rock ratios over a range of pressures is recognized in the form of interstitial Cpx, spinel and/or plagioclase, and magmatic veins (Dick, 1989; Cannat *et al.*, 1992; Constantin *et al.*, 1995; Seyler & Bonatti, 1997; Seyler *et al.*, 2001; Warren *et al.*, 2009). Refertilization by low-volume melts percolating along grain boundaries results in more cryptic forms of refertilization, the signature of which is difficult to detect. However, recent detailed studies, in particular by Seyler and co-workers (Seyler *et al.*, 2001, 2004, 2007; Hellebrand

*et al.*, 2002; Brunelli *et al.*, 2006), have documented that many residual peridotites have undergone low degrees of refertilization, with small enrichments in the most incompatible trace elements, the formation of interstitial Cpx veinlets and/or trace metasomatic phases (e.g. amphibole, apatite and mica). In addition, residual abyssal peridotites are not as LREE depleted as they should be if they have undergone only melt extraction (Hellebrand *et al.*, 2002; Brunelli *et al.*, 2006). Modeling by Brunelli *et al.* (2006) suggested that all depleted peridotites have been weakly refertilized by 0·1–1% instantaneous or partially aggregated melts trapped during melt percolation.

'Residual' peridotite Cpx in this study are strongly depleted in LREE (Fig. 5). Their trace element abundance patterns are consistent with residues of fractional melting (Johnson *et al.*, 1990), possibly followed by a low degree of refertilization (Brunelli *et al.*, 2006). Residual Cpx occur as porphyroclasts 1–5 mm in diameter and with exsolution lamellae. In general, their cores and rims are indistinguishable with respect to trace element abundances (Table 9). Various studies have attempted to constrain whether minerals remain in equilibrium with melt during mantle melting or whether diffusion limits equilibrium (Iwamori, 1992, 1993; Qin, 1992; Van Orman *et al.*, 2002; Cherniak & Liang, 2007). The lack of clear evidence for systematic incompatible element depletion in the rims of Cpx grains relative to the cores indicates that Cpx and melt remained in equilibrium during melt extraction at the SWIR.

Cpx in residual peridotites also occur as interstitial grains of <1 mm size without exsolution lamellae. The elongate morphology of some interstitial grains suggests that they formed by crystallization of melt along grain boundaries; however, the majority are more equant in shape, suggestive of recrystallization during ductile flow in the asthenosphere. Table 9 shows that interstitial grains in residual peridotites have similar compositions to porphyroclast cores. This suggests that the melt from which elongate interstitial Cpx crystallized also re-equilibrated with the porphyroclastic Cpx.

'Metasomatic' Cpx in this study are those with large abundance variations or high concentrations of incompatible elements. Samples with metasomatic Cpx vary from LREE-depleted, residual-type patterns to LREE-enriched patterns over small (<2 cm) length-scales. These variations are taken as evidence of cryptic metasomatism by a percolating melt. The length-scales of the trace element variations are not large enough to be preserved for long times (e.g. >1 Myr) at mantle temperatures, as will be demonstrated below. As there is no evidence for rapid uplift or rapid cooling of the core complexes at the Atlantis II Fracture Zone (John *et al.*, 2004), the metasomatism must be related to shallow-level late-stage magmatic processes in oceanic core complexes; this will be discussed further below.
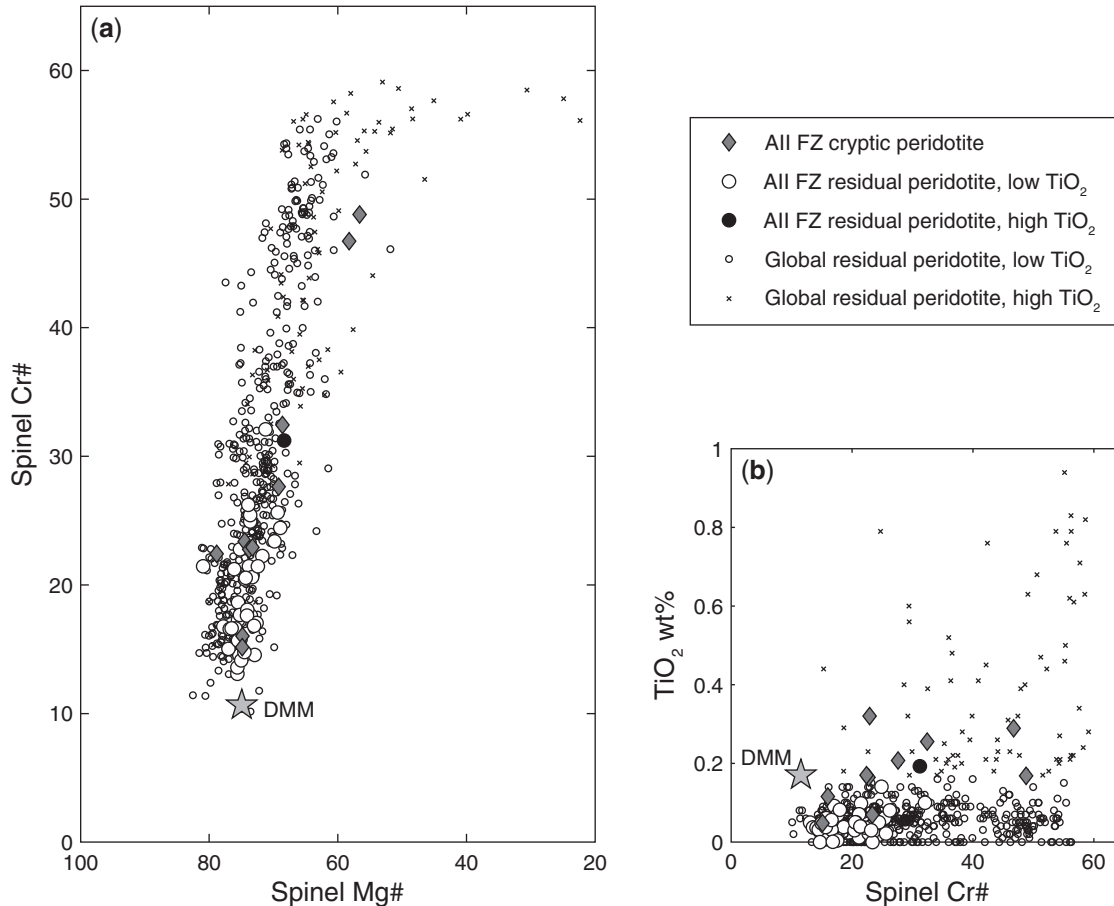
**Fig. 8.** Variations in spinel Cr-number, Mg-number and TiO$_2$ in peridotites from the Atlantis II Fracture Zone compared with the global abyssal peridotite dataset. The cryptically metasomatized peridotites have large variations in spinel Cr-number, Mg-number and TiO$_2$ (Table 6). Additional Atlantis II Fracture Zone data are from Johnson *et al.* (1990), Johnson & Dick (1992), Jaroslow *et al.* (1996), Coogan *et al.* (2004) and Morishita *et al.* (2007); the composition of DMM spinel is from Workman & Hart (2005); the global dataset is from a literature compilation.

Descriptions and models of the interactions of perido-tites with migrating melts and fluids have a long history in studies of mantle metasomatism of the continental litho-sphere (e.g. Menzies *et al.*, 1987; Bodinier & Godard, 2003). Navon & Stolper (1987) and Bodinier *et al.* (1990) were among the first to attempt to explain melt–rock reac-tion in a quantitative fashion. These early models concen-trated on explaining variations among peridotite Cpx trace element patterns and did not include the modal changes that occur during melt–rock reaction. More gen-eralized models that include mineralogical reactions have since been developed (Godard *et al.*, 1995; Vernières *et al.*, 1997).

Particularly interesting and relevant to this study is the chromatographic fractionation of trace elements predicted by these models. As melt percolates around mantle min-erals, fractionation of trace elements occurs because of the differences among mineral–melt partition coefficients for different elements. When an enriched small-degree melt

enters a column of depleted peridotite, the REE patterns of Cpx in the peridotite will be modified successively, beginning with an increase in the most incompatible LREE and progressing towards less incompatible HREE. This process can result in Cpx with 'spoon-shaped' and 'sharply inflected' REE patterns, as observed by Takazawa *et al.* (1992) in depleted lherzolites from the Horoman peri-dotite massif and by Sen *et al.* (1993) in xenoliths from Oahu. In Fig. 6, some Cpx from abyssal peridotite RC27-9-6-5 have inflected 'spoon-shape' REE patterns.

Sample 6K-465-2 illustrates two salient features studied here: first, metasomatism occurs on small length-scales (Figs 2 and 3), and second, the magnitude of metasomatic changes is extremely large for incompatible elements (Fig. 6). In particular, the transition from unmetasoma-tized residual Cpx to completely metasomatized Cpx occurs over a distance of <1 cm (Fig. 2). Zoned Cpx (Fig. 3b) occur only in the transition between depleted (unmetasomatized) and enriched (metasomatized)
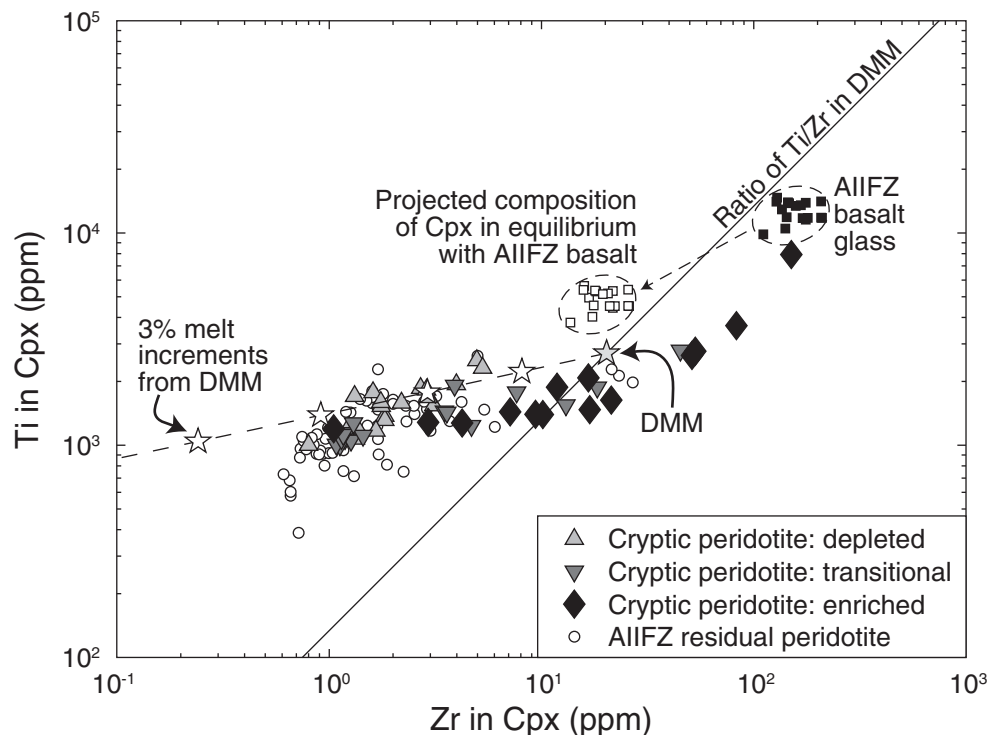
**Fig. 9.** Co-variation of Ti and Zr in peridotite Cpx and basalt glass from the Atlantis II Fracture Zone. Basalt data from Coogan *et al.* (2004); additional Cpx data from Johnson *et al.* (1990) and Johnson & Dick (1992). The melting trend, labeled for 3% fractional melting increments, was calculated using melt modes from Kinzler (1997), partition coefficients from Hart & Dunn (1993) and the composition of Cpx in DMM from Workman & Hart (2005). The continuous line indicates the variation of Ti with Zr at a constant DMM Ti:Zr ratio. Cryptically metasomatized Cpx do not lie on the melting trend and are also not in equilibrium with basalts from the fracture zone.

portions of the rock. These observations suggest that the trace element variations record the metasomatic front. The metasomatized Cpx in Fig. 6 have REE abundances that are compatible with LREE-enriched basalts from the Atlantis II Fracture Zone (Johnson & Dick, 1992), although they would be in equilibrium with melts with slightly higher REE concentrations than are observed.

Figure 9 demonstrates the difference between melting and melt–rock reaction in the depleted versus the metasomatized peridotites. The variation of Zi and Ti in peridotite Cpx was used by Johnson *et al.* (1990) to estimate the degree of melting, as Ti is less incompatible in Cpx than Zr. Depleted peridotites from Atlantis II Fracture Zone follow this general melting trend of decreasing Ti and Zr. In contrast, cryptically metasomatized Cpx do not plot on the fractional melting trend, but instead follow a trend with a shallower slope, indicating that the increase in Zr is greater than that in Ti during metasomatism. Because the Cpx/melt partition coefficient for Zr is smaller than that for Ti, this trend is interpreted as being consistent with the chromatographic effect. A similar observation was made by Tartarotti *et al.* (2002) for Cpx in plagioclase peridotites from the Romanche Fracture Zone. The most enriched Cpx from the Atlantis II peridotites plots close

to the field of basalts from the fracture zone. However, Cpx from the metasomatized peridotites are not in equilibrium with the basalts, indicating that they did not form by direct precipitation from a basaltic melt sampled at the fracture zone.

The cryptically metasomatized peridotites represent the smallest length-scale at which compositional variation has been observed in abyssal peridotites. The REE variations in the cryptic peridotites are similar to the theoretical predictions of chromatographic melt–rock reaction models, for example by Vernières *et al.* (1997). However, given the small size of the samples and the limited spatial information on the exact three-dimensional shape of the zoning front, detailed modeling is precluded at this point. Instead, diffusion calculations are used to place constraints on the timing of cryptic metasomatism. Our diffusion analysis is similar to that employed by Sen *et al.* (2003) for Hawaiian xenoliths, in which they observed small-scale variations in Cpx and plagioclase trace element abundances.

To assess the time-scales for diffusive homogenization, the approximation $x = \sqrt{D_i t}$ is used, where $x$ is distance, $D_i$ is the diffusion coefficient for an element $i$, and $t$ is time. Diffusion coefficients for Ce and Yb in Cpx were

*Table 11: Calculated time-scales for mantle upwelling and diffusive equilibration*

| $T$ (°C) | $\alpha_T$* | $z$ (km) | $t_U$† (Myr) | $P$ (GPa) | $D_{Ce}$‡ (m²/s) | $t_{eq}$ Ce§ ($r = 1$ mm) | $t_{eq}$ Ce ($r = 1$ cm) | $D_{Yb}$‡ (m²/s) | $t_{eq}$ Yb§ ($r = 1$ mm) | $t_{eq}$ Yb ($r = 1$ cm) | $D_{Sr}$** (m²/s) | $t_{eq}$ Sr§ ($r = 1$ mm) | $t_{eq}$ Sr ($r = 1$ cm) |
|---|---|---|---|---|---|---|---|---|---|---|---|---|---|
| 1350 | 10 | 36 | 7 | 1·2 | $4 \times 10^{-20}$ | 0·8 Myr | 80 Myr | $6 \times 10^{-19}$ | 0·05 Myr | 5 Myr | | | |
| 1200 | 5 | 18 | 3 | 0·6 | $2 \times 10^{-21}$ | 20 Myr | 2 Gyr | $4 \times 10^{-20}$ | 0·8 Myr | 80 Myr | $4 \times 10^{-13}$ | 0·08 years | 8 years |
| 1100 | 3·8 | 14 | 2 | 0·5 | $1 \times 10^{-22}$ | 300 Myr | 30 Gyr | $4 \times 10^{-21}$ | 9 Myr | 900 Myr | $9 \times 10^{-17}$ | 400 years | 0·04 Myr |
| 1000 | 3·1 | 11 | 2 | 0·4 | $5 \times 10^{-24}$ | 6 Gyr | 600 Gyr | $2 \times 10^{-22}$ | 140 Myr | 14 Gyr | $1 \times 10^{-18}$ | 30 Kyr | 3 Myr |
| 700 | 1·7 | 6 | 1 | 0·2 | $8 \times 10^{-30}$ | $4 \times 10^{15}$ years | $4 \times 10^{17}$ years | $2 \times 10^{-27}$ | $2 \times 10^{13}$ years | $2 \times 10^{15}$ years | $2 \times 10^{-24}$ | 20 Gyr | 2000 Gyr |

*Scaling factor to calculate the depth to a given isotherm using the equation $L^*_T = \alpha_T \kappa / v_H$, where $\kappa$ is the thermal diffusivity, $10^{-6}$ m²/s, and $v_H$ is the ridge half-spreading rate of 8·7 mm/year from Baines *et al.* (2007). Scaling relation is based on the finite-element model for ridge thermal structure from Montési & Behn (2007).
†Upwelling time from a given isotherm to the seafloor, derived from the scaling relation for depth and the upwelling velocity during ridge corner flow, $v_U = 2v_H / \pi$ (Batchelor, 1967).
‡Diffusion coefficients from Van Orman *et al.* (2001).
§Equilibration time for a grain of 1 mm radius.
¶Equilibration time for a grain of 1 cm radius.
**Diffusion coefficients from Sneeringer *et al.* (1984).

extrapolated from the Van Orman *et al.* (2001) experimental dataset and for Sr from Sneeringer *et al.* (1984). The depth and pressure to a given isotherm beneath the ridge axis, listed in Table 11, were calculated using the scaling relations determined by Montési & Behn (2007), who used a finite-element model to determine ridge thermal structure. Diffusion coefficients in Table 11 were calculated over a temperature range of 700–1350°C. At a given temperature, Sr is the fastest diffusing species in Cpx and Ce the slowest. Over the temperature range of the calculation, the diffusion coefficient for each element varies by many orders of magnitude. For example, at 1350°C, $D_{Ce}$ is $4 \times 10^{-20}$ m²/s, whereas at 700°C, $D_{Ce}$ is $8 \times 10^{-30}$ m²/s (Table 11). Diffusion length-scales have been calculated for Cpx grain radii of 1 mm, the smallest length-scale at which trace elements vary, and at 1 cm, the maximum length-scale of variability. Although 1 cm is larger than the radii of Cpx in this study, it is taken as a proxy for diffusivity across the 2 cm diameter zone over which trace element disequilibrium is observed.

The results of the diffusion calculation are plotted in Fig. 10, which shows the time for diffusive equilibration as a function of temperature for grains of 1 mm and 1 cm radii. The upwelling time from the depth of a given isotherm to the seafloor is also shown in Fig. 10, calculated from the ridge corner flow equation (Table 11). This line separates grain sizes and temperatures where diffusive equilibration of the peridotite can occur within the time-scale of mid-ocean ridge upwelling from those where diffusion is too slow for homogenization. For example, at 700°C and 6 km depth, diffusive equilibration does not occur at either the millimeter or centimeter length-scale (assuming that extrapolation of the diffusion

data to this temperature is valid). In contrast, at 1350°C and 37 km depth, trace element gradients in Cpx at the millimeter to centimeter length scales will diffusively homogenize in 7 Myr. Even though Cpx will also cool during those 7 Myr, slowing diffusion, the calculation indicates that ~1 Myr is sufficient time for diffusive homogenization of all elements. Hence, the variations observed in samples such as 6K-465-2 cannot be preserved if they form at 1350°C, indicating that the metasomatism occurred after the peridotite had cooled below its solidus and adiabatic decompression melting had stopped.

The first-order diffusion calculation can be used to place further constraints on the pressure and temperature of the peridotite metasomatism. The variability of trace element concentrations between the enriched and depleted portions of the peridotite depends on the element, with the more incompatible elements showing larger variability. For example, the average concentration of Ce in the depleted region of sample 6K-465-2 is 0·08 ± 0·09 ppm, whereas in the enriched region it has an average concentration two orders of magnitude higher, 3·46 ± 2·48 ppm. Yb shows less variability, with an average of 1·22 ± 0·31 ppm in the depleted region and 2·69 ± 1·34 ppm in the enriched region. Finally, Sr is relatively homogeneous in the sample, with an average composition in the depleted region of 2·10 ± 1·54 ppm and in the enriched region of 1·64 ± 0·68 ppm. Comparing these observations with Fig. 10, this pattern is best matched if the metasomatism occurred around 1100°C and 14 km depth.

Two of the metasomatized peridotites are from Atlantis Bank on the Atlantis II Fracture Zone. Baines *et al.* (2008) estimated that during formation of Atlantis Bank at
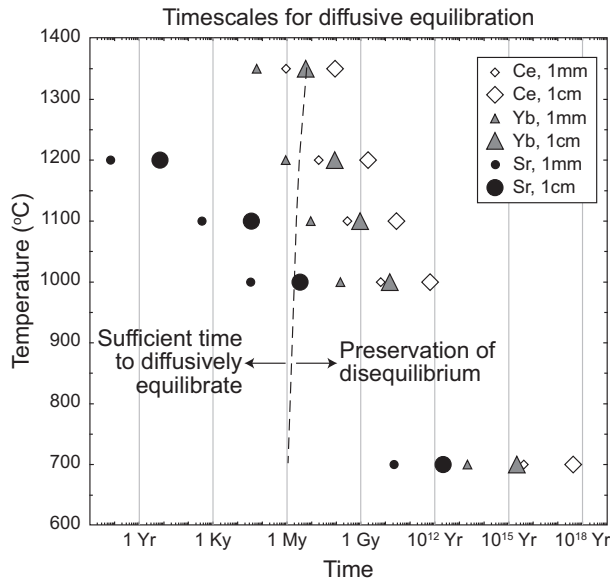
**Fig. 10.** Time-scales for diffusive equilibration of Ce, Yb, and Sr in Cpx as a function of temperature. This calculation is for Cpx with 1 mm radius (smaller symbols) and 1 cm radius (larger symbols), which is equivalent to the minimum and maximum length-scales over which disequilibrium is observed in the metasomatized peridotites. The calculations are based on experimental diffusion datasets from Van Orman *et al.* (2001) for Ce and Yb, and from Sneeringer *et al.* (1984) for Sr. The pressure for the calculations was determined based on the temperature, half-spreading rate, and scaling relations from Montési & Behn (2007) for the thermal structure of an ultraslow-spreading ridge. The dashed line represents the upwelling time to reach the seafloor starting at a given temperature/depth, calculated from the Montési & Behn (2007) scaling relations and the solution for corner flow beneath a ridge axis (Batchelor, 1967).

12 Ma, the full ridge spreading rate was faster and more asymmetrical, with a half-spreading rate to the south of 14·1 mm/year. This is based on analysis of both magnetic isochrons and Pb/U dating of magmatic zircons from Atlantis Bank gabbros. This faster spreading rate indicates faster upwelling and thus less time for diffusive equilibration. Calculating diffusion length scales to match the pressure–temperature profile for this faster spreading rate indicates that for diffusive homogenization of Sr to occur, the metasomatism must have occurred around 1200°C and 10 km depth.

Overall, the trace element data for the four metasomatized peridotites suggest that metasomatism of this type occured at temperatures of ∼1000–1200°C and depths of ∼10–20 km. This implies shallow, late-stage melt infiltration of the lithospheric mantle at the ridge axis, which has cooled below its solidus. Hence, this provides a direct observation that the lithosphere at the ridge axis can have a finite thickness of 10–20 km, unlike standard ridge models where adiabatically upwelling asthenospheric mantle extends (theoretically) to the crust (e.g. Klein & Langmuir, 1987; McKenzie & Bickle, 1988; Kinzler & Grove, 1992).

## Formation of plagioclase in the metasomatized peridotites

Plagioclase is present in trace quantities (<0·01%) in at least two of the four cryptically metasomatized abyssal peridotites. Plagioclase grains are <1 mm diameter and found in association with spinel. Plagioclase may be present in the other two metasomatized peridotites, especially as Cpx in 6K-458-1 have negative Eu anomalies. However, plagioclase is difficult to identify at the trace level, particularly in more altered samples such as 6K-458-1 and 6K-458-3. Plagioclase has not been been found in the 10 depleted peridotites in this study, although Cpx in some of the samples have small negative Eu anomalies, suggesting that plagioclase may be present.

Technically all abyssal peridotites should contain plagioclase, not spinel, as Al-spinel is metastable at shallow depths in the mantle. Around a depth of ∼20–30 km, the high-pressure mineral assemblage should break down via the reaction (Green & Hibberson, 1970; Borghini *et al.*, 2010) Al-Spinel + Clinopyroxene + Orthopyroxene → Plagioclase + Olivine + Cr-Spinel. However, depleted abyssal peridotites are all spinel peridotites. Trace (<0·1%) plagioclase has been identified in only 15% of abyssal peridotites, based on a literature compilation of modal data for 493 depleted abyssal peridotites. The metastability of spinel is partly due to Cr, as Cr-spinel extends the spinel stability field to ∼15 km (Asimow *et al.*, 1995). However, the general lack of plagioclase in depleted abyssal peridotites suggests that there is either a kinetic barrier to spinel breakdown or to plagioclase nucleation.

An alternative explanation for the presence of plagioclase is crystallization from an infiltrating melt. Plagioclase formed by melt impregnation has been documented in abyssal, ophiolitic, orogenic and xenolith peridotites (e.g. Dick, 1989; Seyler & Bonatti, 1997; Dijkstra *et al.*, 2001; Müntener & Piccardo, 2003; Sen *et al.*, 2003; Borghini *et al.*, 2007; Kaczmarek & Müntener, 2008). However, in these examples the amount of plagioclase in peridotites is generally >1% and can approach 20%. Grains often occur as large porphyroclasts, not just small interstitial grains. In contrast, plagioclase in the metasomatized peridotites in this study consist of interstitial grains associated with interstitial olivine at the embayed edges of spinel (Fig. 3d).

Two characteristics of plagioclase grains in the metasomatized peridotites indicate that they are not the result of the melt infiltration events that produced large trace element variations. The first is that plagioclase is found in the depleted, not the enriched, regions of the peridotites (Fig. 2). The second is the pattern of negative Eu anomalies in Cpx that occur when plagioclase is present. These anomalies are due to the preferential partitioning of $Eu^{2+}$ into plagioclase, the only REE that occurs in both 2+ and 3+ valence states. The cores of both enriched and

depleted Cpx generally have no Eu anomaly, whereas the rims of both types of Cpx have negative anomalies. The occurrence of Eu anomalies in Cpx rims but not cores is shown in Fig. 11, by the ratio of Eu* (the predicted Eu concentration calculated from Sm and Dy concentrations) to measured Eu concentration. In the REE patterns in Fig. 5, most Cpx cores in 6K-465-2 and RC27-9-6-5 are observed to have no negative Eu anomaly. It should be noted, however, that in the plot for 6K-465-2, some cores have negative anomalies, which is probably due to the thin section being cut through the rim of these Cpx.

The lack of an Eu anomaly in enriched and depleted Cpx cores, and the presence of a negative anomaly in all Cpx rims, indicates that plagioclase formation occurred after the metasomatism. If plagioclase crystallized during the metasomatic event, then the REE patterns of enriched Cpx cores should have negative Eu anomalies. In contrast, Cpx rims from both depleted and enriched regions of the peridotite have negative Eu anomalies (Fig. 11). Rim depletion in Eu could have occurred if plagioclase formed by spinel breakdown or if it formed by crystallization from a later, low-volume infiltrating melt.

Sr also preferentially partitions into plagioclase; however, Sr concentrations are similar in Cpx cores and rims, and in the enriched and depleted regions of the peridotite. This is probably due to diffusive homogenization, assuming that Sr is faster diffusing than Eu. Although no diffusion data for Eu in Cpx exist, the diffusion coefficient of $Eu^{3+}$ in Cpx can be assumed to be within the REE range (Van Orman *et al.*, 2001). It is also unclear whether Sr has a negative or positive anomaly in the metasomatized peridotites. If the traditional ordering of trace elements is used, then Sr plots as a negative anomaly between Nd and Sm. However, this element order is based on the partitioning of elements into basaltic melt (Hofmann, 1988). Consideration of plagioclase–Cpx partitioning for Sr suggests that in both minerals Sr is more incompatible than La, as a result of its larger ionic radius. Using this ordering of the elements, depleted regions of the peridotites have positive Sr anomalies (with respect to La) and enriched regions have negative Sr anomalies. These apparent anomalies are due to variation in La concentrations, as the average Cpx Sr concentration does not vary between the depleted ($2.56 \pm 1.56$ ppm) and enriched ($2.65 \pm 1.75$ ppm) regions of the peridotites. As discussed in the previous section, the lack of Sr variability suggests that Sr has diffusively equilibrated across the metasomatized peridotites. Plagioclase formation can then be considered to have lowered the Sr concentration of both Cpx cores and rims, as a result of faster diffusion and a Sr Plag/Cpx partition coefficient that is larger for Sr ($\sim$9) than for Eu ($\sim$2), estimated from Wood & Blundy (2003).

Plagioclase with a breakdown origin in abyssal peridotites has rarely been identified. In most examples of
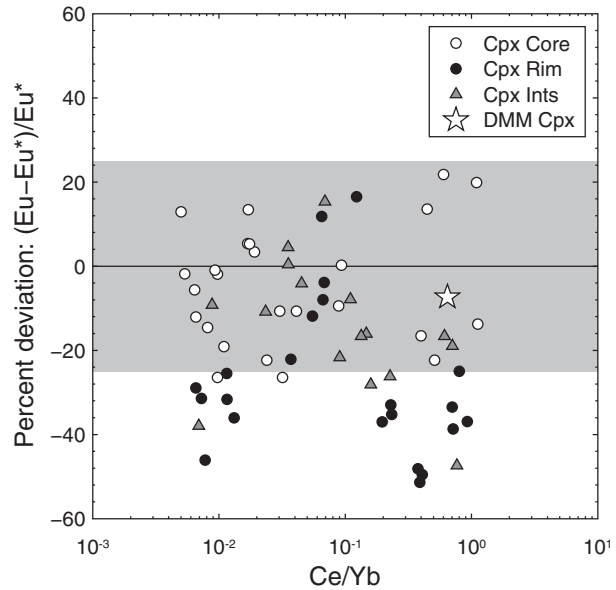


**Fig. 11.** Eu anomalies in Cpx from the cryptically metasomatized peridotites. Ints refers to interstitial Cpx, whereas Core and Rim refer to Cpx porphyroclasts. Eu* is the predicted Eu concentration based on Sm and Dy concentrations in a Cpx grain. The continuous line indicates the absence of an anomaly and the grey shaded box is ±25% error, within which Eu anomalies are not significant. The ratio Ce/Yb provides a measure of the relative depletion or enrichment of Cpx. Rims of Cpx from both depleted and enriched regions of the peridotite have significant negative anomalies (i.e. >−25% deviation), whereas cores and interstitial grains typically have no Eu anomaly.

plagioclase-bearing abyssal peridotites, high modal proportions of plagioclase and relatively fertile compositions indicate a melt origin (e.g. Dick, 1989; Seyler & Bonatti, 1997; Tartarotti *et al.*, 2002). Only two occurrences of abyssal peridotites with breakdown plagioclase have been proposed in the literature: Owen Fracture Zone peridotites on the Central Indian Ridge (Hamlyn & Bonatti, 1980) and Vema Fracture Zone peridotites on the MAR (Cannat & Seyler, 1995). The Owen Fracture Zone example is based on limited major element data with no trace element data, hence the argument for breakdown is inconclusive. The peridotites from the Vema Fracture Zone are mylonites. If the plagioclase formed by breakdown, this could have been caused by the deformation, as has been observed in an orogenic peridotite (Newman *et al.*, 1999). However, without trace element data for these samples, a melt origin for the plagioclase cannot be ruled out in either example.

The characteristics of the plagioclase in the metasomatized peridotites in this study do not exclude a melt origin, although they do require a second, low-volume, melt infiltration event after the first event that created the large variations in Cpx trace elements. The fact that the majority of abyssal peridotites do not contain plagioclase leads

to the question of why breakdown would occur in any samples. If the trace amounts of plagioclase in the samples in this study formed by spinel breakdown, this reaction was probably triggered by the presence of small amounts of melt. Hence, we conclude that plagioclase in the peridotites either crystallized from a small amount of infiltrating melt or breakdown of spinel was triggered by melt. The occurrence of trace plagioclase in any abyssal peridotite may always be related to very small amounts of melt refertilization. Such a conclusion is in agreement with the Cpx trace element modeling of Brunelli et al. (2006), which suggests that all abyssal peridotites have undergone weak refertilization.

Recently, Borghini et al. (2009, 2010) have presented an experimentally derived plagioclase barometer, based on anorthite content and temperature:

$$1{\cdot}05 \; - \; 1{\cdot}71 \; \frac{An}{100} \; + \; 0{\cdot}000686\,T$$

where $P$ is pressure in GPa, An is % anorthite, and $T$ is temperature in °C. As the trace element metasomatism is estimated to have occurred in the temperature range 1000–1200°C, the assumed maximum temperature for plagioclase formation is 1000°C. Average anorthite in 6K-465-2 is 91% and in RC27-9-6-5 is 84% (Table 7). Using a pressure–depth conversion of 1 GPa $\sim$ 30 km, plagioclase is estimated to have a maximum formation depth of 5 km and 9 km, respectively.

## Mid-ocean ridge processes

The observation of multiple shallow-level melt impregnation events in four peridotites from the Atlantis II Fracture Zone suggests that melt–rock interaction in the mantle is considerably more important than previously suggested for this area (Johnson et al., 1990; Johnson & Dick, 1992; Coogan et al., 2004). However, this observation is in agreement with recent models for oceanic core complex formation (e.g. Dick et al., 2000; John et al., 2004; Ildefonse et al., 2007). Further, the observation of melt impregnation agrees with evidence for the importance of melt–rock interaction in the mantle at other slow- and ultraslow-spreading ridges (Seyler et al., 2001, 2004, 2007; Hellebrand et al., 2002; Brunelli et al., 2006). This suggests that the interaction of melts with the mantle through which they migrate is important during the generation of oceanic lithosphere.

Two of the cryptically metasomatized samples (6K-465-2 and RC27-9-6-5) are from the present-day RTI core complex and the other two (6K-458-1 and 6K-458-3) are from the Atlantis Bank fossil core complex, located at 12 Ma along the fracture zone. Oceanic core complexes are uplifted massifs on the seafloor and have been recognized as an important component of the ridge tectonic system (Cann et al., 1997; Tucholke et al., 1998). Spreading at core complexes is accommodated by low-angle detachment faulting. Lower crust and upper mantle are uplifted and exposed on one side of the ridge axis, and the hanging wall of the fault transports the basaltic crust in the opposite direction. Models of oceanic core complexes have proposed that they form at slow-spreading ridges where magma supply is variable (e.g. Escartín et al., 2003; Ildefonse et al., 2007; MacLeod et al., 2009). In these regions, the oceanic lithosphere consists of gabbro intruded into peridotite, which results in strain localization and detachment faulting.

In Fig. 12, sample averaged Cpx REE are plotted for dredges and dives from the Atlantis II Fracture Zone RTI and Atlantis Bank. In addition, single analyses for the cryptically metasomatized peridotites are plotted to demonstrate the large compositional range of these samples. The background light grey field is the range for all other Atlantis II Fracture Zone peridotites along the transform fault (Johnson & Dick, 1992), which is much more limited than the range for the two core complexes. Peridotites from the core complexes extend to REE compositions almost as depleted as the most depleted fracture zone samples, but they also extend to an order of magnitude more enriched compositions than other Atlantis II peridotites. This large range in trace element compositions indicates that other processes, such as magmatic intrusion into the mantle, occur at the Atlantis II Fracture Zone, in addition to depletion by fractional melting. This observation is in agreement with the complex magmatic history that is often inferred for these types of massifs (John et al., 2004; Tucholke et al., 2008).

At Atlantis Bank, extensive surveys of the massif have revealed that a large gabbro body makes up the bulk of the core complex (Dick et al., 2000; John et al., 2004). Gabbro represents 52% of recovered dredge and dive material, in addition to a 1·5 km drill core that is entirely gabbroic (Dick et al., 2000). Analyses of the gabbros have demonstrated the occurrence of several magmatic pulses and magmatic differentiation during the >1 Myr when the core complex was active (Natland & Dick, 2002; John et al., 2004; Baines et al., 2009). At least one other study of Atlantis Bank peridotite has found evidence for melt entrapment in the mantle, in the form of a gabbro veined dunite with cross-cutting chromite within a harzburgite (Morishita et al., 2007).

The presence of a large gabbro body at Atlantis Bank provides a general source for the metasomatism of peridotites 6K-458-1 and 6K-458-3. These peridotites were collected $\sim$250 m apart on Dive 458, although not in situ (Table 1), and other samples recovered in this dive include oxide gabbros. Hence, 6K-458-1 and 6K-458-3 were probably metasomatized by melt squeezed out of nearby gabbro into the surrounding peridotite. Given that the trace element concentrations of 6K-458-1 and 6K-458-3 form a continuous gradation from depleted to enriched (Fig. 12), the
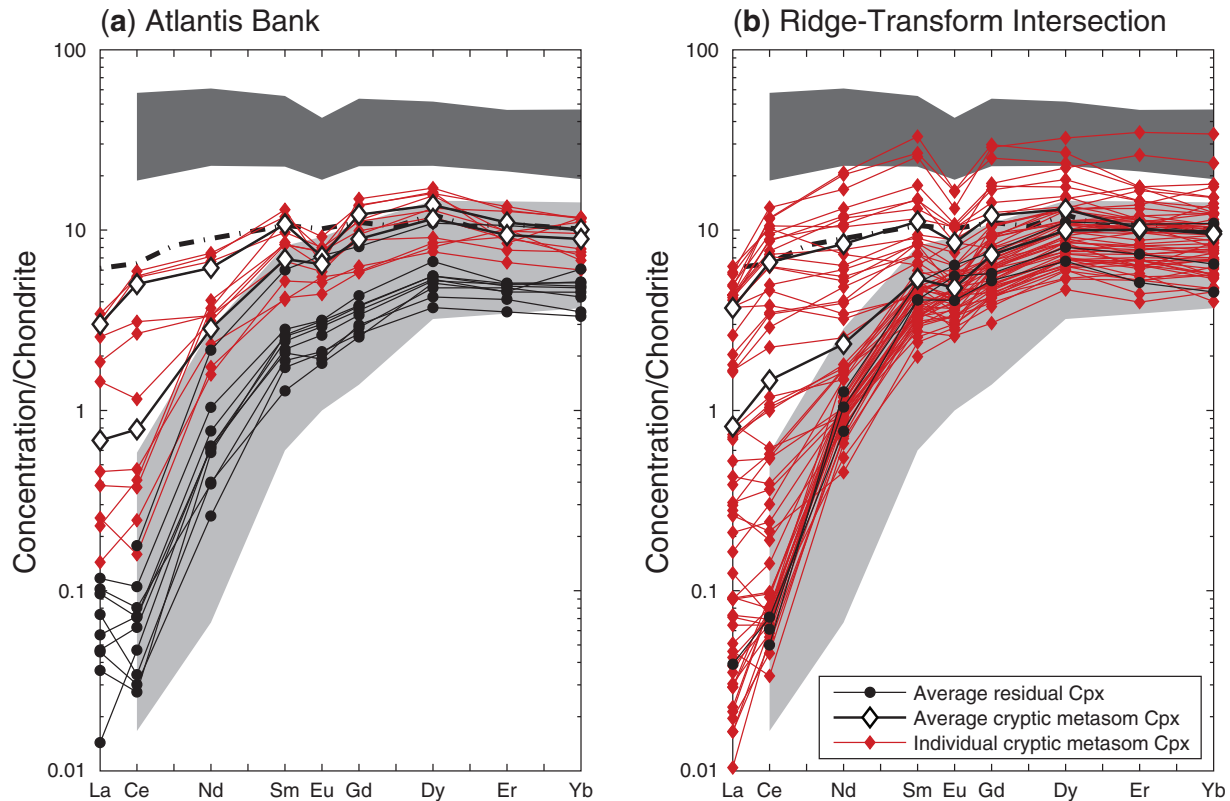
**Fig. 12.** Atlantis II Fracture Zone REE variations at (a) Atlantis Bank and (b) the ridge–transform intersection. Residual peridotites are shown as sample averages. Both average and single analyses are shown for the cryptically metasomatized peridotites. The averages in (a) are for 6K-458-1 and 6K-458-3 and in (b) are for 6K-465-2 and RC27-9-6-5. Data are chondrite normalized (Anders & Grevesse, 1989) and background fields are the Atlantis II Fracture Zone datasets for peridotites (light grey) and basalts (dark grey) from Johnson & Dick (1992).

metasomatism of these samples may have been the result of a single event. However, as the metasomatic Cpx do not have significant Zr or Ti depletions compared with residual Cpx, this suggests that the infiltrating melt was not strongly fractionated. Hence, the oxide gabbros from Dive 458 may not be the source of the melt, but instead represent a later episode of melt intrusion. Zircon and apatite dating by John *et al.* (2004) suggests several cycles of melt intrusion in the gabbro at Atlantis Bank. Gabbro crystallization at Atlantis Bank is estimated to have occurred over a temperature range of 700–1000°C, based on Ti-in-zircon thermometry by Grimes *et al.* (2009). This observation is consistent with our estimate for the first episode of peridotite metasomatism occurring in the range 1000–1200°C, if multiple melt intrusion events occurred and the oxide gabbros formed later in the history of this region of Atlantis Bank.

The RTI at Atlantis II Fracture Zone is considerably less studied and less sampled than Atlantis Bank. The two metasomatized peridotites, RC27-9-6-2 and 6K-465-2, were collected at separate locations (Fig. 1) and must have been metasomatized separately. The composition of plagioclase supports this conclusion, as plagioclase in

RC27-9-6-5 is estimated to have formed at 9 km depth, based on the Borghini *et al.* (2009) barometer, whereas plagioclase in 6K-465-2 has a 5 km depth estimate. At both locations, there is direct evidence for melt intrusion into the mantle, in the form of clinopyroxenite- and gabbro-veined peridotites in Dredge RC27-9-6 and olivine gabbros in Dive 465. Hence, similar to Atlantis Bank, the mantle at the present-day RTI has undergone a long history of melt intrusion into the mantle, which has created heterogeneous lithosphere.

## CONCLUSIONS

Geochemical analyses of abyssal peridotites from the Atlantis II Fracture Zone on the Southwest Indian Ridge reveal the occurrence of cryptic metasomatism in the oceanic lithospheric mantle. Of 14 peridotites analyzed, all appear macroscopically to be residual peridotites, as a result of the absence of cross-cutting veins or dunites. In three samples, Cpx grains with typical, depleted trace element concentrations and those with enriched concentrations occur within 1–2 cm of each other. In a fourth sample, Cpx trace element concentrations are uniformly

enriched. Compared with the composition of typical residual peridotites, these four samples are enriched in LREE by three orders of magnitude. Co-variation of Ti and Zr in the cryptically metasomatized peridotites indicates that the chemical heterogeneity did not result from variable degrees of fractional melting or by direct crystallization from a basaltic melt. Instead, the large variation in trace elements is interpreted to be the result of infiltration by low-volume melt fractions.

This study expands the observational length-scale for variations in abyssal peridotite composition down to the single grain ($\sim$1–5 mm) and single rock ($\sim$10–50 cm) scales. In general, Cpx in abyssal peridotites are not zoned, either within or among grains. The lack of zonation in the majority of abyssal peridotites suggests that diffusion does not limit the equilibration of Cpx with melt during mantle melting. In the metasomatized peridotites, the small spatial scale of the variations can be preserved only if the metasomatism occurred at shallow depth in the lithospheric mantle. Based on calculations of the time-scales for diffusive equilibration, melt impregnation is estimated to have occurred at depths of 10–20 km and temperatures of 1000–1200°C. Hence, the lithospheric mantle at the ridge axis can be relatively thick at ultraslow-spreading ridges.

In at least two of the metasomatized samples, trace amounts of plagioclase ($<$0·01 %) intergrown with spinel, olivine, and pyroxenes are present. Plagioclase may have formed either by crystallizing directly from a low-volume infiltrating melt or by breakdown of spinel triggered by the presence of small amounts of melt. In either case, plagioclase formation post-dates the trace element metasomatic event, as both enriched and depleted Cpx have negative Eu anomalies in their rims but not their cores. This observation suggests that melt–rock reaction occurs multiple times and to shallow depths in the mantle.

The Atlantis II Fracture Zone peridotites in this study are located on oceanic core complexes at the present-day RTI and at Atlantis Bank. At both locations, sampling of veined peridotites and gabbros provides evidence for intrusion of melt into the mantle. In particular, studies of Atlantis Bank have found evidence for a prolonged history of magmatic intrusions. Hence, metasomatism of the peridotites in this study probably relates to various shallow-level intrusions of mafic melts into the lithospheric mantle during oceanic core complex formation. The lithospheric mantle at ultraslow-spreading ridges can thus be relatively heterogeneous in composition.

## ACKNOWLEDGEMENTS

## REFERENCES

Albee, A. L. & Ray, L. (1970). Correction factors for electron probe microanalysis of silicates, oxides, carbonates, phosphates, and sulfates. *Analytical Chemistry* **42**(12), 1408–1414.

Anders, E. & Grevesse, N. (1989). Abundances of the elements: Meteoritic and solar. *Geochimica et Cosmochimica Acta* **53**, 197–214.

Asimow, P. D., Hirschmann, M. M., Ghiorso, M. S., O'Hara, M. J. & Stolper, E. M. (1995). The effect of pressure-induced solid–solid phase transitions on decompression melting of the mantle. *Geochimica et Cosmochimica Acta* **59**(21), 4489–4506.

Baines, A. G., Cheadle, M. J., Dick, H. J. B., Hosford Scheirer, A., John, B. E., Kusznir, N. J. & Matsumoto, T. (2003). Mechanism for generating the anomalous uplift of oceanic core complexes: Atlantis Bank, Southwest Indian Ridge. *Geology* **31**(12), 1105–1108.

Baines, A. G., Cheadle, M. J., Dick, H. J. B., Hosford Scheirer, A., John, B. E., Kusznir, N. J. & Matsumoto, T. (2007). Evolution of the Southwest Indian Ridge from 55°45′E to 62°E: Changes in plate-boundary geometry since 26 Ma. *Geochemistry, Geophysics, Geosystems* **8**(6), doi:10.1029/2006GC001,559.

Baines, A. G., Cheadle, M. J., John, B. E. & Schwartz, J. J. (2008). The rate of oceanic detachment faulting at Atlantis Bank, SW Indian Ridge. *Earth and Planetary Science Letters* **273**, 105–114.

Baines, A. G., Cheadle, M. J., John, B. E., Grimes, C. B., Schwartz, J. J. & Wooden, J. L. (2009). SHRIMP Pb/U zircon ages constrain gabbroic crustal accretion at Atlantis Bank on the ultraslow-spreading Southwest Indian Ridge. *Earth and Planetary Science Letters* **287**, 540–550.

Batchelor, G. K. (1967). *An Introduction to Fluid Dynamics*. Cambridge: Cambridge University Press.

Bence, A. E. & Albee, A. L. (1968). Empirical correction factors for the electron microanalysis of silicates and oxides. *Journal of Geology* **76**, 382–403.

Bodinier, J.-L. & Godard, M. (2003). Orogenic, ophiolitic, and abyssal peridotites. In: Carlson, R. W. (ed.) *Treatise on Geochemistry, Vol. 2*. Amsterdam: Elsevier, pp. 103–170.

Bodinier, J. L., Vasseur, G., Vernières, J., Dupuy, C. & Fabries, J. (1990). Mechanisms of mantle metasomatism: Geochemical evidence from the Lherz orogenic peridotite. *Journal of Petrology* **31**(3), 597–628.

Borghini, G., Rampone, E., Crispini, L., De Ferrari, R. & Godard, M. (2007). Origin and emplacement of ultramafic–mafic intrusions in the Erro–Tobbio mantle peridotite (Ligurian Alps, Italy). *Lithos* **94**, 210–229.

Borghini, G., Fumagalli, P. & Rampone, E. (2009). The composition of plagioclase in mantle peridotites: A geobarometric marker for

lithospheric mantle exhumation. In: Montanini, A., Piccardo, G. B. & Tribuzio, R. (eds) *Alpine Ophiolites and Modern Analogues.* Italy: Università di Parma, Parma, pp. 25–26, wwwalpineophiolite2009 .org.

Borghini, G., Fumagalli, P. & Rampone, E. (2010). The stability of plagioclase in the upper mantle: Subsolidus experiments on fertile and depleted lherzolite. *Journal of Petrology* **50.**

Boudier, F. & Nicolas, A. (1995). Nature of the Moho Transition Zone in the Oman Ophiolite. *Journal of Petrology* **36**(3), 777–796.

Bown, J. W. & White, R. S. (1994). Variation with spreading rate of oceanic crustal thickness and geochemistry. *Earth and Planetary Science Letters* **121**, 435–449.

Brunelli, D., Seyler, M., Cipriani, A., Ottolini, L. & Bonatti, E. (2006). Discontinuous melt extraction and weak refertilization of mantle peridotites at the Vema Lithospheric Section (Mid-Atlantic Ridge). *Journal of Petrology* **47**(4), 745–771.

Cann, J. R., Blackman, D. K., Smith, D. K., McAllister, E., Janssen, B., Mello, S., Avgerinos, E., Pascoe, A. R. & Escartin, J. (1997). Corrugated slip surfaces formed at ridge–transform intersections on the Mid-Atlantic Ridge. *Nature* **385**, 329–332.

Cannat, M. & Seyler, M. (1995). Transform tectonics, metamorphic plagioclase and amphibolitization in ultramafic rocks of the Vema transform fault (Atlantic Ocean). *Earth and Planetary Science Letters* **133**, 283–298.

Cannat, M., Bideau, D. & Hébert, R. (1990). Plastic deformation and magmatic impregnation in serpentinized ultramafic rocks from the Garrett transform fault (East Pacific Rise). *Earth and Planetary Science Letters* **101**, 216–232.

Cannat, M., Bideau, D. & Bougault, H. (1992). Serpentinized peridotites and gabbros in the Mid-Atlantic Ridge axial valley at 15°37′N and 16°52′N. *Earth and Planetary Science Letters* **109**, 87–106.

Cherniak, D. J. & Liang, Y. (2007). Rare earth element diffusion in natural enstatite. *Geochimica et Cosmochimica Acta* **71**, 1324–1340.

Constantin, M. (1999). Gabbroic intrusions and magmatic metasomatism in harzburgites from the Garrett transform fault: Implications for the nature of the mantle–crust transition at fast-spreading ridges. *Contributions to Mineralogy and Petrology* **136**, 111–130.

Constantin, M., Hékinian, R., Ackermand, D. & Stoffers, P. (1995). Mafic and ultramafic intrusions into upper mantle peridotites from fast spreading centers of the Easter Microplate (South East Pacific). In: Vissers, R. L. M. & Nicolas, A. (eds) *Mantle and Lower Crust Exposed in Oceanic Ridges and in Ophiolites.* Dordrecht: Kluwer Academic, pp. 71–120.

Coogan, L. A., Thompson, G. M., MacLeod, C. J., Dick, H. J. B., Edwards, S. J., Hosford Scheirer, A. & Barry, T. L. (2004). A combined basalt and peridotite perspective on 14 million years of melt generation at the Atlantis Bank segment of the Southwest Indian Ridge: Evidence for temporal changes in mantle dynamics. *Chemical Geology* **207**, 13–30.

Dantas, C., Ceuleneer, G., Grégoire, M., Python, M., Freydier, R., Warren, J. & Dick, H. J. B. (2007). Pyroxenites from the Southwest Indian Ridge, 9–16°E: Cumulates from incremental melt fractions produced at the top of a cold melting regime. *Journal of Petrology* **48**(4), 647–660.

Dick, H. J. B. (1989). Abyssal peridotites, very slow spreading ridges and ocean ridge magmatism. In: Saunders, A. D. & Norry, M. J. (eds) *Magmatism in the Ocean Basins.* Geological Society, London, Special Publications **42**, 71–105.

Dick, H. J. B. & Bullen, T. (1984). Chromian spinel as a petrogenetic indicator in abyssal and alpine-type peridotites and spatially associated lavas. *Contributions to Mineralogy and Petrology* **86**, 54–76.

Dick, H. J. B. & Natland, J. H. (1996). Late-stage melt evolution and transport in the shallow mantle beneath the East Pacific Rise. In:

Mével, C., Gillis, K. M., Allan, J. F. & Meyer, P. S. (eds) *Proceedings of the Ocean Drilling Program, Scientific Results, 147.* College Station, TX: Ocean Drilling Program, pp. 103–134.

Dick, H. J. B., Fisher, R. L. & Bryan, W. B. (1984). Mineralogic variability of the uppermost mantle along mid-ocean ridges. *Earth and Planetary Science Letters* **69**, 88–106.

Dick, H. J. B., *et al.* (1991). Tectonic evolution of the Atlantis II Fracture Zone. In: Von Herzen, R. P. & Robinson, P. T. (eds) *Proceedings of the Ocean Drilling Program, Scientific Results, 118.* College Station, TX: Ocean Drilling Program, pp. 359–398.

Dick, H. J. B., Lin, J. & Schouten, H. (2003). An ultraslow-spreading class of ocean ridge. *Nature* **426**, 405–412.

Dick, H. J. B., Lissenberg, C. J. & Warren, J. M. (2010). Mantle melting, melt transport and delivery beneath a slow-spreading ridge: The paleo-MAR from 23°15′N to 23°45′N. *Journal of Petrology* **50.**

Dick, H. J. B., Natland, J. H., *et al.* (2000). A long *in situ* section of the lower ocean crust: Results of ODP Leg 176 drilling at the Southwest Indian Ridge. *Earth and Planetary Science Letters* **179**, 31–51.

Dijkstra, A. H., Drury, M. R. & Vissers, R. L. M. (2001). Structural petrology of plagioclase peridotites in the west Othris Mountains (Greece): Melt impregnation in mantle lithosphere. *Journal of Petrology* **42**, 5–24.

Dijkstra, A. H., Drury, M. R., Vissers, R. L. M. & Newman, J. (2002). On the role of melt–rock reaction in mantle shear zone formation in the Othris Peridotite Massif (Geece). *Journal of Structural Geology* **24**, 1431–1450.

Escartín, J., Mével, C., MacLeod, C. J. & McCaig, A. M. (2003). Constraints on deformation conditions and the origin of oceanic detachments: The Mid-Atlantic Ridge core complex at 15°45′N. *Geochemistry, Geophysics, Geosystems* **4**(8, doi:10.1029/2002GC000,472.

Fujii, T. (1990). Petrology of peridotites from Hole 670A, Leg 109. In: Detrick, R., Honnorez, J., Bryan, W. B., Juteau, T. *et al.* (eds) *Proceedings of the Ocean Drilling Program, Scientific Results, 106/109.* College Station, TX: Ocean Drilling Program, pp. 19–25.

Gaetani, G. A. & Grove, T. L. (1998). The influence of water on melting of mantle peridotite. *Contributions to Mineralogy and Petrology* **131**, 323–346.

Ghose, I., Cannat, M. & Seyler, M. (1996). Transform fault effect on mantle melting in the MARK area (Mid-Atlantic Ridge south of the Kane transform). *Geology* **24**(12), 1139–1142.

Godard, M., Bodinier, J.-L. & Vasseur, G. (1995). Effects of mineralogical reactions on trace element redistributions in mantle rocks during percolation processes: A chromatographic approach. *Earth and Planetary Science Letters* **133**, 449–461.

Green, D. H. & Hibberson, W. (1970). The instability of plagioclase in peridotite at high pressure. *Lithos* **3**(3), 209–221.

Grimes, C. B., John, B. E., Cheadle, M. J., Mazdab, F. K., Wooden, J. L., Swapp, S. & Schwartz, J. J. (2009). On the occurrence, trace element geochemistry, and crystallization history of zircon from *in situ* ocean lithosphere. *Contributions to Mineralogy and Petrology* **158**, 757–783.

Hamlyn, P. R. & Bonatti, E. (1980). Petrology of mantle-derived ultramafics from the Owen Fracture Zone, northwest Indian Ocean: Implications for the nature of the oceanic upper mantle. *Earth and Planetary Science Letters* **48**, 65–79.

Hanghøj, K., Kelemen, P. B., Hassler, D. & Godard, M. (2010). Composition and genesis of depleted mantle peridotites from the Wadi Tayin Massif, Oman Ophiolite. Major and trace element geochemistry, and Os isotope and PGE systematics. *Journal of Petrology* **50.**

Hart, S. R. & Dunn, T. (1993). Experimental cpx/melt partitioning of 24 trace elements. *Contributions to Mineralogy and Petrology* **113**, 1–8.

Hellebrand, E., Snow, J. E., Dick, H. J. B. & Hofmann, A. W. (2001). Coupled major and trace elements as indicators of the extent of melting in mid-ocean-ridge peridotites. *Nature* **410**, 677–681.

Hellebrand, E., Snow, J. E., Hoppe, P. & Hofmann, A. W. (2002). Garnet-field melting and late-stage refertilization in 'residual' abyssal peridotites from the Central Indian Ridge. *Journal of Petrology* **43**(12), 2305–2338.

Hofmann, A. W. (1988). Chemical differentiation of the Earth: The relationship between mantle, continental crust, and oceanic crust. *Earth and Planetary Science Letters* **90**, 297–314.

Hoogerduijn Strating, E. H., Rampone, E., Piccardo, G. B., Drury, M. R. & Vissers, R. L. M. (1993). Subsolidus emplacement of mantle peridotites during incipient oceanic rifting and opening of the Mesozoic Tethys (Voltri Massif, NW Italy). *Journal of Petrology* **34**, 901–927.

Hosford, A., Tivey, M., Matsumoto, T., Dick, H., Schouten, H. & Kinoshita, H. (2003). Crustal magnetization and accretion at the Southwest Indian Ridge near the Atlantis II Fracture Zone, 0–25 Ma. *Journal of Geophysical Research* **108**(B3), doi:10.1029/2001JB000,604.

Ildefonse, B., Blackman, D. K., John, B. E., Ohara, Y., Miller, D. J. & MacLeod, C. J. (2007). Oceanic core complexes and crustal accretion at slow-spreading ridges. *Geology* **35**, 623–626.

Irving, A. J. & Frey, F. A. (1984). Trace element abundances in megacrysts and their host basalts: Constraints on partition coefficients and megacryst genesis. *Geochimica et Cosmochimica Acta* **48**, 1201–1221.

Iwamori, H. (1992). Melt–solid flow with diffusion-controlled chemical reaction. *Geophysical Research Letters* **19**(3), 309–312.

Iwamori, H. (1993). A model for disequilibrium mantle melting incorporating melt transport by porous and channel flows. *Nature* **366**, 734–737.

Jaroslow, G. E., Hirth, G. & Dick, H. J. B. (1996). Abyssal peridotite mylonites: Implications for grain-size sensitive flow and strain localization in the oceanic lithosphere. *Tectonophysics* **256**, 17–37.

Jochum, K. P., Dingwell, D. B., Rocholl, A., Stoll, B., Hofmann, A. W., *et al.* (2000). The preparation and preliminary characterisation of eight geological MPI-DING reference glasses for *in-situ* microanalysis. *Geostandards Newsletter* **24**(1), 87–133.

John, B. E., Foster, D. A., Murphy, J. M., Cheadle, M. J., Baines, A. G., Fanning, C. M. & Copeland, P. (2004). Determining the cooling history of *in situ* lower oceanic crust—Atlantis Bank, SW Indian Ridge. *Earth and Planetary Science Letters* **222**, 145–160.

Johnson, K. T. M. & Dick, H. J. B. (1992). Open system melting and temporal and spatial variation of peridotite and basalt at the Atlantis II Fracture Zone. *Journal of Geophysical Research* **97**(B6), 9219–9241.

Johnson, K. T. M., Dick, H. J. B. & Shimizu, N. (1990). Melting in the oceanic upper mantle: An ion microprobe study of diopsides in abyssal peridotites. *Journal of Geophysical Research* **95**, 2661–2678.

Juteau, T., Berger, E. & Cannat, M. (1990). Serpentinized, residual mantle peridotites from the M.A.R. median valley, ODP Hole 670A (21°10′N, 45°02′W, Leg 109): Primary mineralogy and geothermometry. In: Detrick, R., Honnorez, J., Bryan, W. B., Juteau, T. *et al.* (eds) *Proceedings of the Ocean Drilling Program, Scientific Results, 106/109*. College Station, TX: Ocean Drilling Program, pp. 27–45.

Kaczmarek, M.-A. & Müntener, O. (2008). Juxtaposition of melt impregnation and high-temperature shear zones in the upper mantle; field and petrological constraints from the Lanzo Peridotite (northern Italy). *Journal of Petrology* **49**(12), 2187–2220.

Kelemen, P. B. & Dick, H. J. B. (1995). Focused melt flow and localized deformation in the upper mantle: Juxtaposition of replacive dunite and ductile shear zones in the Josephine peridotite, SW Oregon. *Journal of Geophysical Research* **100**(B1), 423–438.

Kelemen, P. B., Dick, H. J. B. & Quick, J. E. (1992). Formation of harzburgite by pervasive melt/rock reaction in the upper mantle. *Nature* **358**, 635–641.

Kelemen, P. B., Shimizu, N. & Salters, V. J. M. (1995). Extraction of mid-ocean-ridge basalt from the upwelling mantle by focused flow of melt in dunite channels. *Nature* **375**, 747–753.

Kinzler, R. J. (1997). Melting of mantle peridotite at pressures approaching the spinel to garnet transition: Application to mid-ocean ridge basalt petrogenesis. *Journal of Geophysical Research* **102**(B1), 853–874.

Kinzler, R. J. & Grove, T. L. (1992). Primary magmas of mid-ocean ridge basalts 2. Applications. *Journal of Geophysical Research* **97**(B5), 6907–6926.

Klein, E. M. & Langmuir, C. H. (1987). Global correlations of ocean ridge basalt chemistry with axial depth and crustal thickness. *Journal of Geophysical Research* **92**(B8), 8089–8115.

Kumagai, H., Dick, H. J. B. & Kaneoka, I. (2003). Noble gas signatures of abyssal gabbros and peridotites at an Indian Ocean core complex. *Geochemistry, Geophysics, Geosystems* **4**(12), doi:10.1029/2003GC000,540.

Lee, K.-L. (1997). Petrological and geochemical studies of an abyssal peridotite from the Atlantis II Fracture Zone. Master's thesis, MIT/WHOI Joint Program.

Le Roux, V., Bodinier, J.-L., Tommasi, A., Alard, O., Dautria, J. M., Vauchez, A. & Riches, A. J. V. (2007). The Lherz spinel lherzolite: Refertilized rather than pristine mantle. *Earth and Planetary Science Letters* **259**, 599–612.

Liang, Y. (2003). Kinetics of crystal–melt reaction in partially molten silicates: 1. Grain scale processes. *Geochemistry, Geophysics, Geosystems* **4**(5), doi:10.1029/2002GC000,375.

MacLeod, C. J., Searle, R. C., Murton, B. J., Casey, J. F., Mallows, C., Unsworth, S. C., Achenbach, K. L. & Harris, M. (2009). Life cycle of oceanic core complexes. *Earth and Planetary Science Letters* **287**, 333–344.

McKenzie, D. P. & Bickle, M. J. (1988). The volume and composition of melt generated by extension of the lithosphere. *Journal of Petrology* **29**, 625–679.

Menzies, M. A., Rogers, N., Tindle, A. & Hawkesworth, C. J. (1987). Metasomatic and enrichment processes in lithospheric peridotites, an effect of asthenosphere–lithosphere interaction. In: Menzies, M. A. & Hawkesworth, C. J. (eds) *Mantle Metasomatism*. New York: Academic Press, pp. 313–361.

Montési, L. G. J. & Behn, M. D. (2007). Mantle flow and melting underneath oblique and ultraslow mid-ocean ridges. *Geophysical Research Letters* **34**, L24,307, doi:10.1029/2007GL031067.

Morgan, Z., Liang, Y. & Kelemen, P. B. (2008). Significance of the concentration gradients associated with dunite bodies in the Josephine and Trinity ophiolites. *Geochemistry, Geophysics, Geosystems* **9**(7), doi:10.1029/2008GC001954.

Morishita, T., Maeda, J., Miyashita, S., Kumagai, H., Matsumoto, T. & Dick, H. J. B. (2007). Petrology of local concentration of chromian spinel in dunite from the slow-spreading Southwest Indian Ridge. *European Journal of Mineralogy* **19**, 871–882.

Müntener, O. & Piccardo, G. B. (2003). Melt migration in ophiolitic peridotites: the message from Alpine–Apennine peridotites and implications for embryonic ocean basins. In: Dilek, Y. & Robinson, P. T. (eds) *Ophiolites in Earth History. Geological Society, London, Special Publications* **218**, 69–89.

Natland, J. H. & Dick, H. J. B. (2002). Stratigraphy and composition of gabbros drilled in Ocean Drilling Program Hole 735B, Southwest Indian Ridge: A synthesis of geochemical data.

In: Natland, J. H., Dick, H. J. B., Miller, D. J. & Von Herzen, R. P. (eds) *Proceedings of the Ocean Drilling Program, Scientific Results, 176*, pp. 1–69, doi:10.2973/odp.proc.sr.176.002.2002.

Navon, O. & Stolper, E. (1987). Geochemical consequences of melt percolation: The upper mantle as a chromatographic column. *Journal of Geology* **95**, 285–307.

Newman, J., Lamb, W. M., Drury, M. R. & Vissers, R. L. M. (1999). Deformation processes in a peridotite shear zone: Reaction-softening by an $H_2O$-deficient, continuous net transfer reaction. *Tectonophysics* **303**, 193–222.

Python, M. & Ceuleneer, G. (2003). Nature and distribution of dykes and related melt migration structures in the mantle section of the Oman ophiolite. *Geochemistry, Geophysics, Geosystems* **4**(7), doi:10.1029/2002GC000,354.

Qin, Z. (1992). Disequilibrium partial melting model and its implications for trace element fractionations during mantle melting. *Earth and Planetary Science Letters* **112**, 75–90.

Sen, G., Frey, F. A., Shimizu, N. & Leeman, W. P. (1993). Evolution of the lithosphere beneath Oahu, Hawaii: Rare earth element abundances in mantle xenoliths. *Earth and Planetary Science Letters* **119**, 53–69.

Sen, G., Yang, H.-J. & Ducea, M. (2003). Anomalous isotopes and trace element zoning in plagioclase peridotite xenoliths of Oahu (Hawaii): Implications for the Hawaiian plume. *Earth and Planetary Science Letters* **207**, 23–38.

Seyler, M. & Bonatti, E. (1997). Regional-scale melt–rock interaction in lherzolitic mantle in the Romanche Fracture Zone (Atlantic Ocean). *Earth and Planetary Science Letters* **146**, 273–287.

Seyler, M., Toplis, M. J., Lorand, J.-P., Luguet, A. & Cannat, M. (2001). Clinopyroxene microtextures reveal incompletely extracted melts in abyssal peridotites. *Geology* **29**(2), 155–158.

Seyler, M., Lorand, J.-P., Toplis, M. J. & Godard, G. (2004). Asthenospheric metasomatism beneath the mid-ocean ridge: Evidence from depleted abyssal peridotites. *Geology* **32**(4), 301–304.

Seyler, M., Lorand, J.-P., Dick, H. J. B. & Drouin, M. (2007). Pervasive melt percolation reactions in ultra-depleted refractory harzburgites at the Mid-Atlantic Ridge, 15°20′N: ODP Hole 1274A. *Contributions to Mineralogy and Petrology* **153**, 303–319.

Shimizu, N., Semet, M. P. & Allègre, C. J. (1978). Geochemical applications of quantitative ion-microprobe analysis. *Geochimica et Cosmochimica Acta* **42**, 1321–1334.

Sneeringer, M., Hart, S. R. & Shimizu, N. (1984). Strontium and samarium diffusion in diopside. *Geochimica et Cosmochimica Acta* **48**, 1589–1608.

Suhr, G., Hellebrand, E., Snow, J. E. & Seck, H. A. (2003). Significance of large, refractory dunite bodies in the upper mantle

of the Bay of Islands Ophiolite. *Geochemistry, Geophysics, Geosystems* **4**(3), doi:10.1029/2001GC000277.

Takahashi, E. (1986). Melting of a dry peridotite KLB-1 up to 14 GPa: Implications on the origin of peridotitic upper mantle. *Journal of Geophysical Research* **91**(B9), 9367–9382.

Takazawa, E., Frey, F. A., Shimizu, N., Obata, M. & Bodinier, J. L. (1992). Geochemical evidence for melt migration and reaction in the upper mantle. *Nature* **359**, 55–58.

Tartarotti, P., Susini, S., Nimis, P. & Ottolini, L. (2002). Melt migration in the upper mantle along the Romanche Fracture Zone (Equatorial Atlantic). *Lithos* **63**, 125–149.

Tucholke, B. E., Lin, J. & Kleinrock, M. C. (1998). Megamullions and mullion structure defining oceanic metamorphic core complexes on the Mid-Atlantic Ridge. *Journal of Geophysical Research* **103**(B5), 9857–9866.

Tucholke, B. E., Behn, M. D., Buck, W. R. & Lin, J. (2008). Role of melt supply in oceanic detachment faulting and formation of megamullions. *Geology* **36**(6), 455–458.

Van der Wal, D. & Bodinier, J.-L. (1996). Origin of the recrystallisation front in the Ronda peridotite by km-scale pervasive porous melt flow. *Contributions to Mineralogy and Petrology* **122**, 387–405.

Van Orman, J. A., Grove, T. L. & Shimizu, N. (2001). Rare earth element diffusion in diopside: Influence of temperature, pressure, ionic radius, and an elastic model for diffusion in silicates. *Contributions to Mineralogy and Petrology* **141**, 687–703.

Van Orman, J. A., Grove, T. L. & Shimizu, N. (2002). Diffusive fractionation of trace elements during production and transport of melt in Earth's upper mantle. *Earth and Planetary Science Letters* **198**, 93–112.

Vernières, J., Godard, M. & Bodinier, J.-L. (1997). A plate model for the simulation of trace element fractionation during partial melting and magma transport in the Earth's upper mantle. *Journal of Geophysical Research* **102**(B11), 2471–24,784.

Warren, J. M., Shimizu, N., Sakaguchi, C., Dick, H. J. B. & Nakamura, E. (2009). An assessment of upper mantle heterogeneity based on abyssal peridotite isotopic compositions. *Journal of Geophysical Research* **114**(B12203), doi:10.1029/2008JB006186.

Wood, B. J. & Blundy, J. D. (2003). Trace element partitioning under crustal and uppermost mantle conditions: The influences of ionic radius, cation charge, pressure, and temperature. In: Carlson, R. W. (ed.) *Treatise on Geochemistry, Vol. 2*. Amsterdam: Elsevier, pp. 395–424.

Workman, R. K. & Hart, S. R. (2005). Major and trace element composition of the depleted MORB mantle (DMM). *Earth and Planetary Science Letters* **231**, 53–72.